Monthly Notices
of the
ROYAL ASTRONOMICAL SOCIETY

MNRAS **432,** 3186–3217 (2013) doi:10.1093/mnras/stt673
Advance Access publication 2013 May 21

Symbiotic stars and other Hα emission-line stars towards the Galactic bulge⋆

Brent Miszalski,[1,2]† Joanna Mikołajewska[3] and Andrzej Udalski[4]

[1]*South African Astronomical Observatory, PO Box 9, Observatory 7935, South Africa*
[2]*Southern African Large Telescope Foundation, PO Box 9, Observatory 7935, South Africa*
[3]*Nicolaus Copernicus Astronomical Centre, Bartycka 18, PL-00716 Warsaw, Poland*
[4]*Warsaw University Observatory, Al. Ujazdowskie 4, PL-00-478 Warsaw, Poland*

Accepted 2013 April 17. Received 2013 April 1; in original form 2013 March 1

ABSTRACT

Symbiotic stars are interacting binaries with the longest orbital periods, and their multicomponent structure makes them rich astrophysical laboratories. The accretion of a high-mass-loss-rate red giant wind on to a white dwarf (WD) makes them promising Type Ia supernova (SN Ia) progenitors. Systematic surveys for new Galactic symbiotic stars are critical to identify new promising SN Ia progenitors (e.g. RS Oph) and to better estimate the total population size to compare against SN Ia rates. Central to the latter objective is building a complete census of symbiotic stars towards the Galactic bulge. Here we report on the results of a systematic survey of Hα emission-line stars covering 35 deg^2. It is distinguished by the combination of deep optical spectroscopy and long-term light curves that improve the certainty of our classifications. A total of 20 bona fide symbiotic stars are found (13 S-types, 6 D-types and 1 D′-type), 35 per cent of which show the symbiotic specific Raman-scattered O VI emission bands, as well as 15 possible symbiotic stars that require further study (six S-types and nine D-types). Light curves show a diverse range of variability including stellar pulsations (semi-regular and Mira), orbital variations and slow changes due to dust. Orbital periods are determined for five S-types and Mira pulsation periods for three D-types. The most significant D-type found is H1-45 and its carbon Mira with a pulsation period of 408.6 d, corresponding to an estimated period–luminosity relation distance of ∼6.2 ± 1.4 kpc and $M_K = -8.06 \pm 0.12$ mag. If H1-45 belongs to the Galactic bulge, then it would be the first bona fide luminous carbon star to be identified in the Galactic bulge population. The lack of luminous carbon stars in the bulge is a longstanding unsolved problem. A possible explanation for H1-45 may be that the carbon enhancement was accreted from the progenitor of the WD companion. A wide variety of unusual emission-line stars were also identified. These include central stars of planetary nebulae (PNe) [one (WC10-11) Wolf–Rayet and five with high-density cores], two novae, two WN6 Wolf–Rayet stars, two possible Be stars, a B[e] star with a bipolar outflow, an ultracompact H II region and a dMe flare star. Dust obscuration events were found in two central stars of PNe, increasing the known cases to five, as well as one WN6 star. There is considerable scope to uncover several more symbiotic stars towards the bulge, many of which are currently misclassified as PNe, provided that deep spectroscopy is combined with optical and near-infrared light curves.

Key words: surveys – binaries: symbiotic – stars: carbon – stars: emission-line, Be – planetary nebulae: general – Galaxy: bulge.

⋆Based on observations made with the Anglo-Australian Telescope (AAT) at Siding Spring Observatory, the 1.3 m Warsaw Telescope at Las Campanas Observatory of the Carnegie Institution for Science, Chile, the Very Large Telescope (VLT) at Paranal Observatory under programme 079.D-0764(A), the Southern African Large Telescope (SALT) under programme 2012-1-RSA-009, the New Technology Telescope (NTT) at La Silla Observatory under programmes 071.D-0448(A) and 079.D-0764(B), and the South African Astronomical Observatory (SAAO) 1.9 and 1.0 m telescopes.

† E-mail: brent@saao.ac.za

1 INTRODUCTION

Symbiotic stars are the longest orbital period interacting binaries composed of an evolved cool giant and an accreting hot, luminous companion (usually a white dwarf, WD) surrounded by a dense ionized nebula. Depending on the nature of the cool giant, two main classes of symbiotic stars have been defined: S-types (stellar) with normal M giants, and orbital periods of the order of a few years, and D-types (dusty) with Mira primaries surrounded by a warm dust (Whitelock 1987). They host a rich circumstellar environment produced by the ionization of the giant's high-mass-loss-rate wind by the WD. Several phenomena are observed including ionized and neutral regions, dust-forming regions, accretion/excretion discs, interacting winds, and bipolar outflows and jets (see e.g. Mikołajewska 2007, 2012 for recent reviews).

Symbiotic stars have obvious implications towards understanding all interacting binaries that include either evolved giants or accreting WDs during any phase of their evolution. In particular, understanding symbiotic stars may also help to solve one of the timeliest problems in modern astrophysics – the missing progenitors of Type Ia supernovae (SNe Ia). Although there is general consensus that they result from thermonuclear disruption of a CO WD reaching the Chandrasekhar mass, due to either mass accretion from a non-degenerate companion (single-degenerate or SD model) or mass transfer between and/or merger of two WDs (double-degenerate or DD model), the progenitors of SNe Ia have never been observed before the explosion, and each of the proposed scenarios has its strengths and weaknesses (Di Stefano, Orio & Moe 2013, and references therein). In regard to this problem, symbiotic stars are important not only to the SD scenario, where the progenitor is most likely a symbiotic nova similar to RS Oph (e.g. Dilday et al. 2012), but also to the DD scenario since most DD binaries are descended from symbiotic stars (e.g. Di Stefano 2010).

There are two main factors which drive the discovery for more symbiotic stars. First, the potential to find other case studies like RS Oph, and in particular, ensuring that the most interesting objects are routinely monitored for nova-like activity (e.g. those with evidence for tidally distorted donors or orbital periods $\lesssim$1000 d; Mikołajewska 2013). Second, to derive more realistic estimates of the total Galactic symbiotic population and, in turn, to compare symbiotic star birth rates against SN Ia rates. Corradi et al. (2010a) and Corradi (2012) identified the Galactic bulge symbiotic stars as a fundamental population to better characterize before estimates of the total number of Galactic symbiotics can be refined. Current estimates vary considerably from 3×10^3 (Allen 1984), 3×10^4 (Kenyon et al. 1993) to 3–4 $\times 10^5$ (Munari & Renzini 1992; Magrini, Corradi & Munari 2003). None of these, however, are in agreement with the very small number of observed symbiotic stars. Several major catalogues have been compiled including Allen (1984), Kenyon (1986), Mikołajewska, Acker & Stenholm (1997) and Belczyński et al. (2000). These efforts have amounted to no more than ∼300 symbiotics currently known. More recently, ∼1200 symbiotic star candidates were identified from the INT Photometric Hα Survey of the Northern Galactic Plane (IPHAS; Drew et al. 2005). A spectroscopic follow-up campaign of the sample has so far identified 14 new symbiotic stars (Corradi et al. 2008, 2010a,b, 2011; Corradi & Giammanco 2010; Corradi 2012).

A comparable resource to IPHAS in the southern Galactic plane is the AAO/UKST SuperCOSMOS Hα Survey (SHS; Parker et al. 2005). The quantitative colour–colour candidate selection method developed by Corradi et al. (2008) is however problematic to adapt to the photographic SHS data whose colour–colour plane possesses a greater intrinsic dispersion than IPHAS. The Macquarie/AAO/Strasbourg Hα (MASH) planetary nebula (PN) surveys effectively used difference imaging (Parker et al. 2006) and semi-automated techniques (Miszalski et al. 2008) to identify unresolved SHS Hα emitters (e.g. compact PNe, symbiotic stars and other emission-line stars). As the MASH surveys were primarily concerned with PNe, mostly those Hα emitters with the highest chance of being a PN were observed spectroscopically, leaving considerable scope for new symbiotic star discoveries.

Miszalski et al. (2009a) carefully selected a large sample of SHS Hα emitters across ∼35 square degrees towards the Galactic bulge and observed them using the AAOmega spectrograph (Sharp et al. 2006) with the Two-degree Field (2dF) facility on the 3.9 m AAT (Lewis et al. 2002). A preliminary list of candidate symbiotic stars was published by Miszalski et al. (2009a); however, only basic supporting information was given per object as the focus was only to flag non-PNe. A similar approach to that of Miszalski et al. (2009a) was taken in the Large Magellanic Cloud (LMC) by Miszalski et al. (2011c) where some promising symbiotic star candidates were identified.

This paper contains a comprehensive reanalysis of the Hα emitter survey that incorporates deep spectroscopy and long-term *I*-band light curves to identify new symbiotic stars and other unusual Hα emission-line stars. It is structured as follows. Section 2 describes the selection of Hα emission-line candidates and the spectroscopic and photometric observations of the sample. The overall properties and analysis of the sample are discussed in Section 3. A subset of the sample are discussed individually in Sections 4 (new S-type symbiotics), 5 (new D-type symbiotics), 6 (a new D′-type symbiotic), 7 (possible S-type symbiotics) and 8 (possible D-type symbiotics). Objects that were found not to be symbiotic stars are also discussed individually in Sections 9 [high-density core (HDC) PNe], 10 (miscellaneous objects) and in Appendix E (superpositions). Section 11 discusses the completeness and depth of our survey, possible X-ray detections, the unique carbon Mira of H1-45 and its significance in carbon star formation, as well as the common tendencies as a function of symbiotic star type. We conclude in Section 12, and several appendices contain finder charts and other observations of the sample.

2 OBSERVATIONS

2.1 Multi-object spectroscopy

We employ the same multi-object spectroscopy observations previously described by Miszalski et al. (2009a). The main observations were conducted in service mode (PI: Miszalski) using the 4 m AAT with the 2dF/AAOmega facility (Lewis et al. 2002; Sharp et al. 2006) that can allocate up to 392 optical fibres of diameter 2.1 arcsec to science targets over a 2.°1 diameter field of view. Additional observations were made using the 8.2 m VLT with the FLAMES facility (Pasquini et al. 2002) in visitor mode under programme ID 079.D-0764(A). FLAMES was used in the miniature integral field unit (mini-IFU) mode that can allocate up to 15 mini-IFUs for both science and sky targets over a 12.5 arcmin field of view. Each mini-IFU consists of a lenslet array that measures 2 × 3 arcsec^2 which feeds 20 fibres with a spatial sampling of 0.5 arcsec per lenslet.

Tables 1 and 2 give the field centres of 2dF/AAOmega and VLT FLAMES observations where most fibres were allocated to PNe to determine whether such observations were appropriate for measuring their nebular chemical abundances (Miszalski 2009) and

Table 1. Log of AAOmega field centres observed.

Field	ℓ (deg)	b (deg)	Coords (J2000)	Date (dd/mm/yy)	Exposures (s)	JD-245 0000	N(sky)
N2	357.86	+1.86	17 33 09.8 −29 45 12	26/03/07	3×300, 3×1200	4186	73
S3	355.89	−3.26	17 48 44.4 −34 08 30	27/03/07	60, 2×300, 2×1200	4187	60
S18	1.02	−1.59	17 54 15.6 −28 52 25	29/05/08	60, 240, 1800	4616	183
S20	2.28	−3.26	18 03 42.8 −28 36 39	29/05/08	60, 240, 1800	4616	100
S21	3.57	−2.06	18 01 51.1 −26 54 25	29/05/08	60, 240, 1800	4616	100
S22	0.46	−3.72	18 01 26.4 −30 25 37	30/05/08	60, 240, 1800	4617	100
N3	359.72	+1.79	17 38 01.8 −28 14 06	30/05/08	60, 240, 1800	4617	100
N4	1.87	+1.76	17 43 15.0 −26 25 08	30/05/08	60, 240, 1800	4617	100
N5	358.93	+3.80	17 28 26.5 −27 47 56	30/05/08	60, 240, 1800	4617	100
N7	355.32	+2.81	17 22 57.1 −31 20 39	30/05/08	60, 240, 1800	4617	100
S21a	3.47	−2.26	18 02 24.2 −27 05 05	18/04/09	900, 2×1200	4940	25
S3a	355.89	−3.26	17 48 44.4 −34 08 30	19/04/09	300, 5×900	4941	25
S20a	2.18	−2.95	18 02 15.9 −28 32 58	23/04/09	60, 300, 900, 1800	4945	196

Table 2. Log of VLT FLAMES field centres observed that appear in this work. Exposure times are given per grating setting.

Field	ℓ (deg)	b (deg)	Coords (J2000)	Date (dd/mm/yy)	LR1 (s)	LR2 (s)	LR3 (s)	LR5 (s)	LR6 (s)	LR7 (s)	JD-245 0000
F54	357.04	+4.48	17 21 06.0 −28 58 53	10/06/07	1200	1200	300, 1200	1200	600	300	4261
F157	4.07	−3.17	18 07 17.8 −27 00 25	11/06/07	1800	600, 3600	120, 1800	1800	120, 900	600	4262

the remainder to Hα emission-line candidates. Field centres were chosen to maximize the number of catalogued PNe in each field. Most AAOmega fields were observed with a large number of sky fibres (last column of Table 1) to assist in subtracting the highly variable sky background. Targets for spare fibres were chosen by inspection of full-resolution imaging data from the SHS and SuperCOSMOS Sky Survey (SSS; Hambly et al. 2001). Fields were inspected for Hα emitters by blinking a colour-composite image made of SHS Hα (red), SHS short-red (green) and SSS B_J (blue) with the continuum-divided or 'quotient' image (Hα divided by short-red). This approach was first developed during the MASH-II survey (Miszalski et al. 2008).

The prepared target lists for AAOmega fields were allocated fibres with the CONFIGURE program (Shortridge, Ramage & Farrell 2006) that uses a simulated annealing algorithm to achieve an optimal configuration (Miszalski et al. 2006). FLAMES fields were configured using FPOSS, a European Southern Observatory (ESO) adapted version of CONFIGURE, that we customized to show angular deviation limits for mini-IFU fibres to assist in field centre selection. The 580V and 385R volume-phase holographic AAOmega gratings provided a wavelength coverage of 3700–8850 Å at resolutions of 3.5 and 5.3 Å (full width at half-maximum, FWHM), respectively. Miszalski et al. (2011a) gave details of the six grating settings used for the FLAMES observations, made at an average resolving power of $R \sim 12\,000$, in addition to an account of the full data reduction procedure which includes relative flux calibration that we also applied to field F54. AAOmega data were reduced using the 2DFDR program (see e.g. Croom et al. 2005). A typical spectrophotometric response function included with 2DFDR for each spectrograph arm was divided through all data to remove the large-scale instrumental signature. This is by no means an accurate flux calibration since the inherent response of each fibre is different to the next and highly variable. The AAOmega spectra are therefore only useful for classification purposes and line ratios over small-wavelength ranges. Some targets required manual tweaking of their spectra to resubtract background sky spectra minimizing the sky residuals, resplice blue and red arm spectra, interpolate over cosmetic defects (particularly in the blue arm) and to stack multiple exposures. If more than one spectrum is available, then we have chosen to present only a representative spectrum (typically the average of multiple exposures), unless specified otherwise.

2.2 Additional spectroscopy

Parker et al. (2006) published online spectroscopy of PPA 1752−3542 and PPA 1807−3158. An additional two objects were observed separate to the multi-object spectroscopy campaigns. We selected K2-17 (PN G336.8−07.2; Kohoutek 1977) for study because we identified an Hα excess from the central star (CS) in SHS data, while Hen2-375 (PN G337.3−18.3; Henize 1967) appeared to be a good symbiotic star candidate with a red excess in the Two Micron All Sky Survey or 2MASS ($J - K_s = 2.5$ mag; Skrutskie et al. 2006). We observed K2-17 with the SALT (Buckley, Swart & Meiring 2006; O'Donoghue et al. 2006) under programme 2012-1-RSA-009 and Hen2-375 with the SAAO 1.9 m telescope. Table 3 summarizes the observations taken with the Robert Stobie Spectrograph (RSS; Burgh et al. 2003; Kobulnicky et al. 2003) on SALT and the grating spectrograph (SpCCD) on the 1.9 m telescope. Basic pipeline calibrations were applied to the RSS data with the PYSALT[1] package (Crawford et al. 2010), and a relative flux calibration was made with the spectrophotometric standard star LTT7987 (Hamuy et al. 1994). The separate red and blue spectra of the CS of K2-17 were extracted with the APALL IRAF task and joined by matching the stellar continuum. In addition, the brightest part of the K2-17 nebula on the slit was extracted using a 20 arcsec wide aperture, equal in both red and blue spectra, with both spectra joined using the same scale factor for the CS spectrum. The Hen2-375 spectra were reduced in the usual fashion with IRAF and flux calibrated using the CS of NGC 7293 (Oke 1990).

[1] http://pysalt.salt.ac.za

Table 3. Log of SALT RSS and SAAO 1.9 m SpCCD observations.

Object	Spectrograph	Date (dd/mm/yy)	Grating	Exp. time (s)	Slit width (")	λ (Å)	Δλ (FWHM, Å)	Dispersion (Å pixel^{-1})	PA (°)
K2-17	RSS	25/05/12	PG1300	2100	1.5	4275–6365	3.9	0.67	0
K2-17	RSS	20/06/12	PG900	1350	1.5	5880–8880	5.5	0.96	0
Hen2-375	SpCCD	28/06/12	6	3×90, 1200	1.5	4055–5950	2.8	1.10	90
Hen2-375	SpCCD	28/06/12	6	60, 1800	1.5	5710–7560	2.5	1.05	90

2.3 OGLE and MACHO light curves

Several fields towards the Galactic bulge have been extensively monitored by the OGLE[2] (see e.g. Udalski 2009) and MACHO (Alcock et al. 1997) projects at optical wavelengths. Such light curves are ideally suited to study symbiotic stars that demonstrate a rich variety of variability over time-scales of several hundred days including pulsations from the red giant component, ellipsoidal variability or eclipses due to orbital motion and dust obscuration events (Mikołajewska 2001; Gromadzki et al. 2009). This rich legacy data set has only recently been used to study symbiotic stars towards the Galactic bulge (Miszalski et al. 2009a, the precursor to this work; Gromadzki et al. 2009; Lutz et al. 2010) and the Magellanic Clouds (Miszalski et al. 2011c; Kato, Hachisu & Mikołajewska 2013). In particular, they offer significant advantages in distinguishing symbiotic stars apart from PNe (Miszalski et al. 2009a, 2011c). Archival photographic plates also offer substantial opportunities to obtain long baseline light curves (Munari, Jurdana-Šepić & Moro 2001; Munari & Jurdana-Šepić 2002; Jurdana-Šepić & Munari 2010).

We retrieved MACHO light curves from the recently updated virtual observatory compatible website.[3] The MACHO catalogues were overlaid on top of available imaging to select the light curve corresponding to each source (referenced by their MACHO FTS number). Instrumental MACHO magnitudes were transformed into V and R magnitudes using the transformations given in Lutz et al. (2010) after Bessell & Germany (1999).

The procedure was more involved to gather the OGLE photometry which can originate from one or more of the four separate phases of the project. Compared to later OGLE phases, the OGLE-I phase had a more limited survey footprint and sparser sampling (Udalski et al. 1992). For simplicity we include only the OGLE-I light curve of PHR 1806−2652 (Pigulski, Kolaczkowski & Kopacki 2003), relying mostly on the much better sampled OGLE-II (Udalski, Kubiak & Szymański 1997; Szymański 2005), OGLE-III (Udalski et al. 2002a,b, 2008; Szymański et al. 2011) and OGLE-IV (e.g. Poleski et al. 2011; Udalski et al. 2012) photometry. Photometry from the OGLE-IV phase included in this work is somewhat preliminary, coming from the first two to three years of operations, and comes without a finalized photometric scale tied to OGLE-II and OGLE-III photometry. Where possible we attempted to put the OGLE-IV photometry on the OGLE-II/III system based on bright, non-variable stars overlapping between OGLE-III and OGLE-IV fields. This did not always work successfully, most likely because of uncharacterized systematic effects from the OGLE-IV photometry. Colour-related effects may also have played a role where a large spread in stellar $V-I$ colours appears in observed fields, not to mention that many objects in our sample are highly variable and very red ($V-I>2.0$ mag). In most cases, a mean offset from the OGLE-III light curve was estimated and applied to the OGLE-IV light curve. This was more difficult to do in the case of light curves with large-amplitude semi-regular (S-types) or Mira (D-types) pulsations where the mean level is difficult to judge.

[2] http://ogle.astrouw.edu.pl
[3] http://macho.anu.edu.au

3 THE SAMPLE

3.1 Classification

Table 4 gives the names and coordinates of 20 new and 15 possible symbiotic stars that were classified as S-type or D-type (column 3) following the criteria in Belczyński et al. (2000). These criteria include the following.

(a) Detection of the late-type giant (e.g. TiO, Ca II, etc. absorption lines).
(b) Detection of strong emission lines of H I and He I, together with emission lines of higher ionization potential than 35 eV (e.g. [O III]).
(c) Detection of the Raman-scattered O VI emission complex at λλ6825, 7082 (Schmid 1989).

Note that (c) is a sufficient but not necessary condition as only symbiotics with the hottest WDs will be capable of producing this feature. Furthermore, the O VI bands may be redshifted by a fewangstroms (Schmid 1989). Generally, the combination of (a) and (b) is sufficient to classify an object as a symbiotic star. A smaller class of D′-type symbiotics, characterized by G-type giants with clear G bands, absent TiO bands and often carbon enrichment (Mürset & Schmid 1999; Schmid & Nussbaumer 1993). Only one D′ symbiotic was found in our sample (Section 6.1).

Columns 4 and 5 of Table 4 give the AAOmega (Table 1) or FLAMES (Table 2) field names used to observe the source, and the figure numbers in which the spectra appear in this paper. In column 6, the observed Hα/Hβ ratios are given. In the cases where an upper limit is present, the Hβ emission line was coincident with a bad CCD column which reduced the measured Hβ flux. The $E(B-V)$ reddening derived from these ratios under Case B conditions (Brocklehurst 1971) is given in column 7, but these values come with two strong caveats: (a) the accuracy is limited to 0.3–0.5 dex at best by the very poor AAOmega spectrophotometry, and (b) Case B conditions are not necessarily suitable for the very high electron densities encountered in symbiotic stars (e.g. Proga, Mikołajewska & Kenyon 1994; Gutierrez-Moreno, Moreno & Cortes 1995; Luna & Costa 2005). Two exceptions are K2-17 and Hen2-375 with good quality long-slit spectrophotometry. Column 8 gives an estimate of the $E(B-V)$ reddening based on the intrinsic NIR colours of the red giant, as determined from the observed spectral type (see Section 3.3).

Finally, the last column of Table 4 specifies whether the object is surrounded by a resolved nebula. Nebulae are rather common amongst symbiotic stars and are thought to originate from an interaction between the red giant wind and the photoionizing wind of the WD (see e.g. Corradi 1995, 2003; Corradi et al. 1999). Many

Table 4. New and possible symbiotic stars.

Name	Coords (J2000)	Type	Field	Fig.	Hα/Hβ	$E(B-V)$ (Case B)	$E(B-V)$ (NIR)	Nebula present
000.49−01.45	17 52 31.2 −29 15 34	S	S18	1	268.5	4.2	1.6–2.0	–
001.70−03.67	18 04 04.9 −29 18 46	S	S20 S20a	1	6.2	0.7	0.6	–
002.86−01.88	17 59 34.8 −27 25 43	S	S21 S21a	1	–	–	1.5	–
003.46−01.92	18 01 06.3 −26 55 59	S	S21 S21a	2	59.3	2.8	1.3	–
354.98−02.87	17 44 53.0 −34 42 40	D	S3 S3a	6	11.2	1.3	–	–
355.28−03.15	17 46 48.2 −34 36 03	S	S3 S3a	2	37.3	2.4	0.9	–
355.39−02.63	17 44 55.7 −34 14 18	S	S3 S3a	2	27.2	2.1	1.1	–
356.04+03.20	17 23 21.2 −30 31 35	S	N7	3	<87.8	<3.2	1.2	–
357.32+01.97	17 31 23.2 −30 08 44	S	N2	3	51.0	2.7	1.8	–
357.98+01.57	17 34 35.5 −29 48 22	S	N2	3	<98.9	<3.3	1.2	–
358.46+03.54	17 28 13.1 −28 19 38	S	N5	4	28.5	2.1	0.3	–
359.76+01.15	17 40 34.6 −28 31 41	S	N3	4	183.0	3.8	2.5	–
H1-45	17 58 21.8 −28 14 52	D	S20a	6	6.1	0.7	2.2	N
Hen2-375	18 18 09.1 −57 11 14	D	–	6	4.1	0.3	–	Y
JaSt2-6	17 50 01.9 −29 33 25	D	–	–	–	–	6.0	Y
JaSt79	17 51 53.5 −29 30 53	D	S18	7	43.6	2.5	3.0	–
K5-33	17 44 29.9 −27 20 40	D	S3 S3a	7	42.7	2.5	–	–
NSV 22840	17 35 58.5 −28 49 54	S	N3	4	45.6	2.6	2.0	–
PHR 1757−2718	17 57 32.5 −27 18 25	S	S21	5	55.5	2.7	1.8	–
ShWi5	18 03 53.7 −29 51 22	D′	S22	9	10.6	1.2	–	–
001.33+01.07	17 44 37.8 −27 14 17	S?	N4	B1	216.3	4.0	2.2	–
001.37−01.15	17 53 21.2 −28 20 47	D?	S18	B3	362.1	4.5	–	–
001.71+01.14	17 45 13.6 −26 52 42	S?	N4	B1	–	–	1.2	–
001.97+02.41	17 41 02.1 −25 59 34	S?	N4	B1	77.6	3.0	2.1	–
355.12+03.82	17 18 32.2 −30 55 44	S?	N7	B2	14.86	1.5	–	–
357.12+01.66	17 32 04.8 −30 28 55	D?	N2	B3	125.3	3.5	–	–
Al2-B	17 27 47.0 −28 11 03	D?	N5	B3	13.8:	1.5	–	–
Al2-G	17 32 22.6 −28 14 29	D?	N5	B4	22.6	1.9	–	–
M2-24	18 02 02.9 −34 27 47	D?	–	(*a*)	6.2	0.7	–	Y
PHR 1751−3349	17 51 15.0 −33 49 11	D?	S3 S3a	B4	28.7	2.1	–	Y
PHR 1803−2746	18 03 05.0 −27 46 44	D?	S20 S20a S21 S21a	B4	32.4	2.2	–	–
PPA 1746−3454	17 46 51.4 −34 54 05	D?	S3 S3a	B5	25.4	2.0	–	–
PPA 1752−3542	17 52 05.9 −35 42 06	S?	–	(*b*)	–	–	–	–
PPA 1807−3158	18 07 19.1 −31 58 08	D?	–	(*b*)	–	–	–	–
Th3-9	17 23 59.2 −31 01 51	S?	N7	B2	–	–	–	–

(*a*) Zhang & Liu (2003); (*b*) Parker et al. (2006).

of these resolved nebulae were identified from Figs D3–D7 that display colour-composite finder charts of each target in our sample made from SHS/SSS and 2MASS imaging. In some cases, nebulae were also visible on their OGLE finder charts (Figs D1 and D2). Additional imaging sources are specified in the detailed sections on the relevant objects.

Table 5 contains the same information as Table 4 for the non-symbiotic sample except for the reddening derived from the spectral type which is no longer defined. Two objects, M2-29 and PHR 1805−2659, were largely dealt with in Miszalski et al. (2009a, 2011a), but Section 9 also discusses M2-29 in relation to similar objects. Four objects in Table 5 are superpositions and are discussed separately in Appendix E. Section 10 discusses the remainder of the objects in Table 5.

The NIR colour–colour plane has been extensively applied in an attempt to separate symbiotic stars from other samples, especially PNe (e.g. Schmeja & Kimeswenger 2001; Mikołajewska 2004; Corradi et al. 2008). As our sample was Hα selected, the NIR properties were only considered at a later stage and do not bias our survey. The classification of our sample was based mainly on the assessment of spectroscopic features and *I*-band variability (Section 3.2), with NIR properties only later considered to characterize the symbiotic type. Tables A1 and A2 contain near- and mid-infrared magnitudes of our sample collated from the 2MASS (Skrutskie et al. 2006) and the Galactic Legacy Infrared Mid-Plane Survey Extraordinaire (GLIMPSE; see Benjamin et al. 2003, Churchwell et al. 2009) VizieR catalogue (II/293/glimpse), respectively. Inspection of the GLIMPSE images themselves showed the sample to consist entirely of point sources meaning no recourse to aperture photometry was required to determine accurate magnitudes.

3.2 Light curves

Tables 6 and 7 summarize the available light curves for the symbiotic (Table 6) and non-symbiotic (Table 7) samples. Column 3 gives the figure numbers in which the light curves appear in this paper.[4] The MACHO light curves are grouped together, whereas the OGLE light curves are mostly displayed according to what OGLE phases were available as specified in column 4. Column 5 uniquely

[4] Some of these light curves also appear in the long-period variable catalogue of Soszyński et al. (2013).

Table 5. Other objects.

Name	Coords (J2000)	Type	Field	Fig.	Hα/Hβ	$E(B-V)$ (Case B)	Nebula present
003.16−02.31	18 01 56.2 –27 22 55	Nova	S21 S21a	B6	–	–	–
359.88−03.58	17 59 35.6 –30 51 32	WN6	S22	B6	–	–	–
H2-32	17 56 24.2 –29 38 07	Be?	S18	B6	19.9	1.8	–
K2-17	17 09 35.8 –52 13 02	HDC PN	–	10	4.1	0.3	Y
M1-44	18 16 17.3 –27 04 33	PN (superposition)	–	–	–	–	Y
M2-11	17 20 33.4 –29 00 38	HDC PN	F54	10	–	–	Y
M2-29	18 06 40.8 –26 54 56	HDC PN	F157 S21a	(*c*)	5.8	0.7	Y
M3-8	17 24 52.1 –28 05 55	PN (superposition)	N5	(*b*)	–	–	–
M3-38	17 21 04.6 –29 02 59	HDC PN	F54	11	–	–	Y
M4-4	17 28 50.3 –30 07 45	PN (superposition)	N2	E1	–	–	Y
MPA 1746−3412	17 46 18.5 –34 12 37	[WC10-11]	S3 S3a	B7	12.9	1.4	–
PHR 1803−2748	18 03 31.2 –27 48 27	B[e]	S20 S20a S21 S21a	B7	30.0	2.2	Y
PHR 1805−2659	18 05 43.5 –26 59 46	dMe	S21 S21a	(*a*)	4.4	0.4	–
PHR 1806−2652	18 06 56.0 –26 52 54	HDC PN	F157 S21a	11	8.7	1.5	Y
PPA 1758−2628	17 58 37.0 –26 28 47	UCHII	S21 S21a	B7	334.0	4.4	–
PPA 1808−2700	18 08 01.4 –27 00 16	PN (superposition)	F157	E1	–	–	Y
Sa3-104	17 58 25.9 –29 20 48	Be?	S18	B8	16.9	1.6	–
Th3-28	17 30 56.8 –26 59 10	WN6	N5	B8	–	–	–
V4579 Sgr	18 03 37.9 –28 00 07	Nova	S20 S20a S21a	B8	–	–	–

(*a*) Miszalski et al. (2009a). (*b*) Miszalski et al. (2009b). (*c*) Miszalski et al. (2011a).

Table 6. Light-curve information for new and possible symbiotic stars.

Name	Type	Fig.	OGLE	MACHO FTS	$I_{\rm min}$ (JD-245 0000)	Period (d)	Description
000.49−01.45	S	C2	III, IV	–	3736.4	1014.5	Semi-regular pulsations + orbital
001.70−03.67	S	C8	–	114.20492.26	–	–	Flat?
002.86−01.88	S	C2	III, IV	–	4442.6	1068.4	Semi-regular pulsations + orbital
003.46−01.92	S	C2	III, IV	–	4560.2	801.0	Semi-regular pulsations + orbital
354.98−02.87	D	C6	IV	–	–	–	Relatively flat
355.28−03.15	S	C1	II, III, IV	–	–	–	Semi-regular pulsations
355.39−02.63	S	C2	III, IV	–	4431.4	854.5	Semi-regular pulsations + orbital
357.98+01.57	S	C6	IV	–	–	–	Semi-regular pulsations
358.46+03.54	S	C6	IV	–	–	–	Semi-regular pulsations
H1-45	D	C3, C8	III	401.48290.73	3551.0	408.6	Carbon Mira pulsations
JaSt2-6	D	C1	II, III, IV	–	2760.9	605.4	Mira pulsations
JaSt79	D	C3	III, IV	–	3835.4	424.8	Mira pulsations
K5-33	D	C7	IV	–	–	–	Flat
NSV 22840	S	C7	IV	–	–	–	Semi-regular pulsations
PHR 1757−2718	S	C7	IV	–	5634.9	585.0	Semi-regular pulsations + orbital?
ShWi5	D′	C1, C8	I, II, III, IV	119.20354.128	–	–	Low-amplitude orbital?
001.33+01.07	S?	C6	IV	–	–	–	Semi-regular pulsations
001.37−01.15	D?	C6	IV	–	–	–	Relatively flat
001.71+01.14	S?	C6	IV	–	–	–	Semi-regular pulsations
Al2-B	D?	C7	IV	–	–	–	Relatively flat
Al2-G	D?	C7	IV	–	–	–	Slow variations
M2-24	D?	C4	III	–	–	–	Slow variations
PHR 1751−3349	D?	C4	III, IV	–	–	–	Slow large amplitude variations
PHR 1803−2746	D?	C4	III, IV	–	–	–	Relatively flat
PPA 1746−3454	D?	C1	I, II, III, IV	–	–	–	Slow large amplitude variations
PPA 1752−3542	S?	C4	III	–	–	–	Semi-regular pulsations + orbital?
PPA 1807−3158	D?	C5	III, IV	–	–	–	Slow variations

identifies each MACHO light curve in the online archive.[5] Finder charts for OGLE sources may be found in Figs D1 and D2. These may be compared against the images in Figs D3–D7, but note the very different resolutions (0.26 arcsec pixel^{-1} of OGLE versus ∼1 arcsec pixel^{-1} of SHS/SSS). Periodicities were searched for using the phase dispersion minimization (Stellingwerf 1978) IRAF task and the PERIOD04[6] Fourier analysis package (e.g. Lenz & Breger 2004). In some S-type systems, the periodic signature was found

[5] http://macho.anu.edu.au

[6] http://www.univie.ac.at/tops/Period04

Table 7. Light-curve information for other objects.

Name	Type	Fig.	OGLE	MACHO FTS	I_{min} (JD-245 0000)	Period (d)	Description
003.16−02.31	Nova	C2, C8	III	176.19611.10	–	–	Declining
359.88−03.58	WN6	C3	III, IV	–	–	–	Dust obscuration event
H2-32	Be?	14, C3, C8	III, IV	403.47850.5641	–	–	Slow long term + short term
M2-29	HDC PN	(*b*)	I, II, III	101.21568.184	–	–	Dust obscuration event
MPA 1746−3412	[WC10-11]	C3	III, IV	–	–	–	Dust obscuration events
PHR 1803−2748	B[e]	C4, C8	III, IV	104.20254.1855	–	–	Slow variations
PHR 1805−2659	dMe	(*a*), C8	III	101.21176.282	–	–	Flare outbursts
PHR 1806−2652	HDC PN	13	I, II, III	–	–	–	Dust obscuration events
Sa3-104	Be?	C1	II, III, IV	–	–	–	Flat (spurious)
V4579 Sgr	Nova	C5, C8	III, IV	104.20251.191	–	–	Declining

(*a*) Miszalski et al. (2009a). (*b*) Miszalski et al. (2011a).

by inspection. In periodic systems we determined ephemerides by fitting several measured times of minima with a linear ephemeris (see columns 6 and 7 of Table 6). No strictly periodic sources were found amongst non-symbiotic sources. The average time span varies in the ranges 1.5–2.4 (OGLE-IV only), 7.6–10.4 (OGLE-III and OGLE-IV), 14.3–14.6 (OGLE-II to OGLE-IV) and 18.6 yr (OGLE-I to OGLE-IV). The last column in Tables 6 and 7 describes the variability seen in each light curve.

3.3 Cool component spectral types and reddening

Table 8 lists the spectral types of red giant components that were determined for a subset of our sample. We used the indices of Kenyon & Fernandez-Castro (1987) which measure the depth of the VO band at λ7865 ([VO]) and TiO bands at λ6180 Å ($[TiO]_1$) and λ7100 Å ($[TiO]_2$). Also given is the [Na I] index, which although more sensitive to luminosity is useful when combined with the other indices. These indices are based on measurements over fairly small-wavelength ranges of ∼400–650 Å and are suitable for our AAOmega spectra. Apart from H1-45 and ShWi5, only sources with TiO and VO bands strong enough for a reliable classification were included in Table 8. It is well known that these indices give earlier spectral types with decreasing wavelength in symbiotic stars (Kenyon & Fernandez-Castro 1987; Mürset & Schmid 1999). We therefore give classifications for each index, noting that TiO and VO are best suited to types later than K5 and M2, respectively. The last column in Table 8 gives our best estimate of the spectral type which we adopt for the rest of the paper. Additionally, in the case of 355.39−02.63, 357.98+01.57, 358.46+03.54, 359.76+01.15 and PHR 1757−2718, the presence of fairly strong TiO 8432 in their NIR spectra indicates the presence of an M4-5 giant or later, and such a late spectral type was adopted in the reddening estimates below. In D-types, the TiO bands are usually very faint or invisible, leading to very unreliable classifications. In the case of the carbon Mira of H1-45, we used the Richer (1971) scheme to determine a spectral type of C4-7.

Table 8. Spectral classifications of red giant components of new and possible symbiotic stars.

Name	Type	$[TiO]_1$	$[TiO]_2$	[VO]	[Na I]	Adopted
000.49−01.45	S	M0	M3.5	M6	≳M6	M4-6
001.70−03.67	S	K5	M0	M2.5	K/M	K5-M1
002.86−01.88	S	K5	M1	M5.5	M4-5	M4-5
003.46−01.92	S	K5.5	M0.5	M4.5	≳M5	M4-5
355.28−03.15	S	M6	M6	M7	≳M6	M6
355.39−02.63	S	K5.5	M2	M5	≳M5	M2-5
356.04+03.20	S	M4	M5.5	M6	≳M6	M6
357.32+01.97	S	M0.5	M0.5	M2:	K5-M3	M0-1
357.98+01.57	S	M0	M1.5	M5	≳M5	M2-6
358.46+03.54	S	M0.5	M3.5	M6	≳M5	M4-6
359.76+01.15	S	K5	K5	M3	M4-5	M3
H1-45	D	ND	ND	ND	ND	C4-7
NSV 22840	S	M0	M0	M3.5	M0-3	M0-3
PHR 1757−2718	S	M0	M1	M4	≳M5	M1-4
ShWi5	D′	ND	ND	ND	ND	CN
001.33+01.07	S?	M4	M4	M6	M4-6	M4-6
001.71+01.14	S?	ND	M6	M6	≳M6	M6
001.97+02.41	S?	M1	M1	M2:	K/M	M1

ND: Not detected.

We can now estimate the reddening to each object in Table 8 from 2MASS colours (Tables A1 and A2) by comparing the observed $J-K_s$ colour against the intrinsic value. In the case of S-type systems, their intrinsic colours were taken from those of M giants in the Galactic bulge (Feast, Whitelock & Carter 1990). For the D-types with known Mira pulsation periods, their intrinsic colours were estimated using the period–colour relations from Whitelock, Marang & Feast (2000) and Whitelock et al. (2006) for O-rich and C-rich Miras, respectively. In the case of JaSt2-6 and JaSt79, the reddening estimates assume an O-rich Mira. The resultant reddenings are included in column 8 of Table 4. The few Mira variables included in this subsample show reddenings derived from this method that are higher than that derived from the Balmer decrement. This is a well-known fact since in D-type symbiotics, the WD companion and the surrounding ionized region are located outside the Mira's dust shell. This effect is best studied in RX Pup (Mikołajewska et al. 1999) where the reddening towards the Mira is highly variable due to changes in dust shell opacity due to dust obscuration events, whereas the reddening towards the hot ionized region is constant and consistent with the measured interstellar reddening. See also table 3 of Mikołajewska et al. (1997) and section 3 of Mikołajewska (1999).

3.4 Spectroscopic features and temperature estimates of the hot component

Tables 9 and 10 summarize the main observed features in the continuum and the main emission lines present. For Table 9 we have included simple estimates of the hot component temperature T_h based on the highest ionization potential emission lines visible in the spectrum according to Mürset & Nussbaumer (1994). This technique gives a lower limit to the true temperature since we may not see all high-ionization lines. Where possible, we also give the line

Table 9. Description of the continuum, including absorption-line features, estimates of the hot component temperatures T_h and emission-line features present in new and possible symbiotic stars.

Name	Type	Continuum/absorption features	T_h (kK)	Main emission features
000.49−01.45	S	TiO	100	H I, He I, [Fe VII], O I, Ca II triplet
001.70−03.67	S	TiO, Na I D, He I (P Cygni), Ca II K	55	H I, He I, He II, [O III], [O II], O I, Fe II, [Fe II]
002.86−01.88	S	TiO, Na I D	114	H I, He I, O VI
003.46−01.92	S	TiO, Na I D	>55	H I, He I, He II, [O III], O I
354.98−02.87	D	None	114	H I, He I, He II, [O III], [Ne III]
355.28−03.15	S	TiO, Na I D	35	H I, He I, [O III]
355.39−02.63	S	TiO	114	H I, He I, O VI, [Fe VII], O I, Ca II triplet
356.04+03.20	S	TiO, Na I D	114	H I, He I, O VI, He II, [Fe VII]
357.32+01.97	S	TiO, Ca II triplet, Na I D	>55	H I, He I, He II, O I
357.98+01.57	S	TiO	55	H I, He I, He II, [O III], O I
358.46+03.54	S	TiO, Na I D	114	H I, He I, He II, [O III], O VI
359.76+01.15	S	TiO, Na I D	35	H I, He I, [O III], O I, Ca II triplet
H1-45	D	CN, Ba II, Na I D	100	H I, He II, [O III], [Ne III]
Hen2-375	D	None	114	H I, He I, He II, [O III], [Fe VII], O VI
JaSt2-6	D	–	–	–
JaSt79	D	TiO	100	H I, He I, He II, [Fe VII], [Ar V], [O I], [O II], [O III], [Ar III]
K5-33	D	None	114	H I, He I, He II, O VI, [Fe VII], [O III], [Ne III], [Ar III], [Ar IV], [Ar V]
NSV 22840	S	TiO, Na I D	>55	H I, He I, He II, [O III], O I
PHR 1757−2718	S	TiO	114	H I, He I, He II, [Fe VII], O VI, O I, Ca II triplet
ShWi5	D′	CN, CH, Na I D, Ba II 6495	100	H I, He I, He II, [Fe VII], [O III], [Ne III], [Ar III], [Ar IV], [Ar V], [N II]
001.33+01.07	S?	TiO, Na I D	25	H I, He I, O I, Ca II triplet
001.37−01.15	D?	Red	25	H I, He I, [N II], O I, [O I], [O II], Ca II triplet, [S III]
001.71+01.14	S?	TiO	25	H I, He I, Ca II triplet
001.97+02.41	S?	TiO, Ca II triplet, Na I D	25	H I, He I
355.12+03.82	S?	TiO, Na I D	25	H I, He I?, [O I]
357.12+01.66	D?	Na I D	14	O I, H I
Al2-B	D?	(*a*)	41	H I, He I, He II, [O III], [Ne III], [Ar III]
Al2-G	D?	Red	60	H I, He I, He II, [O III], [Ar V], [N II], [Ne III], [Ar III]
M2-24	D?	None	46	H I, He I, [N II], [O III], [Ne III], [Ar IV]
PHR 1751−3349	D?	Weak	25	H I, [N II], O I, [O I], [O II], He I, [S II]
PHR 1803−2746	D?	(*b*)	41	H I, He I, [O III], [Ne III], [Ar III], [O II], [N II], [O I]
PPA 1746−3454	D?	Weak	35	H I, [O III], [N II], [S II], He I, O I
PPA 1752−3542	S?	–	35	H I, [O III]
PPA 1807−3158	D?	–	–	H I, [N II]
Th3-9	S?	Red, Ca II triplet, Na I D	25	H I, He I

(*a*) Continuum is not real and comes from a neighbouring fibre.
(*b*) Continuum is not real and comes from a nearby star.

ratios of [O III] λ4363/Hγ, [O III] λ5007/Hβ and He II λ4686/Hβ for reference in Tables 11 and 12. Such ratios are useful in diagnostic diagrams (e.g. Gutierrez-Moreno et al. 1995). No reddening correction was applied to the ratios.

4 NEW S-TYPE SYMBIOTIC STARS

Figs 1–5 present the spectra of the new S-type symbiotic systems.

4.1 000.49−01.45

The presence of high-ionization [Fe VII] emission lines in the AAOmega spectrum (Fig. 1) ensures the symbiotic nature of this object. The *I*-band light curve in Fig. C2 is typical of an S-type system with an M5-6 giant, namely semi-regular pulsations on top of a probable orbital variability of 1014.5 d.

4.2 001.70−03.67

This is one of the brightest symbiotics in our sample ($J = 9.0$ mag) with a rich emission-line spectrum on top of an K5-M1 red giant (Table 8). It is saturated in the OGLE photometry and the MACHO light curves are rather noisy, making it difficult to derive any conclusion about variability.

4.3 002.86−01.88

This is another significantly reddened S-type symbiotic as proven by the presence of the Raman-scattered O VI 6825 feature. As in the other S-type symbiotics with late M-type red giants, the OGLE light curve (Fig. C2) is dominated by low-amplitude semi-regular pulsations. A longer scale orbital variation of ∼1068.4 d seems to be present. The spectrum shown in Fig. 1 corresponds to the first AAOmega observation which shows the Raman-scattered O VI feature, albeit with a lack of corresponding high-ionization features (e.g. [O III], [Fe VII]). The O VI feature subsequently vanished in the second AAOmega observation 324 d later.

4.4 003.46−01.92

We find an orbital period of 801.0 d from the OGLE light curve that closely resembles that of AR Pav (Rutkowski, Mikołajewska &

Table 10. Description of the continuum, including absorption-line features and emission-line features present in other objects.

Name	Type	Continuum/absorption features	Main emission features
003.16−02.31	Nova	Na I D	He II, N III, [Fe VII], C IV
359.88−03.58	WN6	Na I D	He II, N III, C IV
H2-32	Be?	Na I D, Ca II H & K	H I, O I, [S II], [O I], [O II], [O III], Fe II
K2-17	HDC PN	Blue	H I, He I, He II, [O III], Ca II triplet, [Fe VII], C IV, [Ar V]
M1-44	PN (superposition)	–	–
M2-11	HDC PN	Na I D	[Fe VII]
M2-29	HDC PN	Of(H)	H I, He I, [O III], [Ne III], [Ar III], [N II], [S II], [O II]
M3-8	PN (superposition)	–	–
M3-38	HDC PN	None	[Fe VII]
M4-4	PN (superposition)	–	–
MPA 1746−3412	[WC10-11]	(*a*)	H I, [N II], [S II], C II, C III
PHR 1803−2748	B[e]	Red, Na I D	H I, O I, [O II], [Ni II], [O III], [Fe II], Fe II, [N II]
PHR 1805−2659	dMe	dM	H I, Ca II H&K
PHR 1806−2652	HDC PN	Weak	[Fe VII]
PPA 1758−2628	UCHII	Red	H I, He I, [O III], [O II], [O I], [N II]
PPA 1808−2700	PN (superposition)	–	–
Sa3-104	Be?	Weak, Ca II H&K, Na I D, Hβ	H I, He I, [O III], [O II], [Ar III], [N II], [S III], [S II]
Th3-28	WN6	Red	He II, N III, C IV, N IV, He I
V4579 Sgr	Nova	Blue, Ca II H&K, Na I D	He II, N III, [Fe VII], C IV

(*a*) Continuum is not real and comes from a nearby star.

Table 11. Line ratios of new and possible symbiotic stars.

Name	Type	λ4363/Hγ	λ5007/Hβ	λ4686/Hβ
001.70−03.67	S	0.03	0.15	0.06
003.46−01.92	S	0.67	1.22	0.18
354.98−02.87	D	2.04	2.28	0.07
355.28−03.15	S	0.70	1.50	–
355.39−02.63	S	0.11	0.45	0.50
356.04+03.20	S	–	–	0.87
357.32+01.97	S	0.24	0.14	0.26
357.98+01.57	S	0.42	–	(*a*)
358.46+03.54	S	1.36	1.61	0.30
359.76+01.15	S	–	0.40	–
H1-45	D	1.26	6.88	0.30
Hen2-375	D	2.49	5.37	0.27
JaSt79	D	1.38	11.15	0.53
K5-33	D	2.11	8.35	0.27
NSV 22840	S	0.30	0.51	0.18
PHR 1757−2718	S	–	–	1.18
ShWi5	D′	1.49	9.81	0.35
Al2-B	D?	1.56	11.43	0.10
Al2-G	D?	2.70	8.27	0.20
M2-24	D?	1.41	3.69	0.01
PPA 1746−3454	D?	0.55	0.93	–
PPA 1752−3542	S?	1.80	2.70	–
PHR 1803−2746	D?	3.02	8.07	0.04

(*a*) He II λ4686 detected, but Hβ is affected by bad column on CCD.

Table 12. Line ratios of other objects.

Name	Type	λ4363/Hγ	λ5007/Hβ	λ4686/Hβ
H2-32	Be?	–	0.07	–
K2-17	HDC PN	0.91	0.55	0.68
M2-11	HDC PN	0.69	13.94	0.46
M2-29	HDC PN	1.00	4.00	–
M3-38	HDC PN	0.59	18.09	0.33
PHR 1806−2652	HDC PN	0.10	4.05	0.36
PPA 1758−2628	UCHII	–	18.37	–
Sa3-104	Be?	0.47	1.63	–

Whitelock 2007). The eclipsing binary shows a probable secondary minimum indicative of ellipsoidal variability.

4.5 355.28−03.15

There is no He II λ4686 in the AAOmega spectrum; however, strong [O III] and He I emission lines support its symbiotic nature. The combined OGLE light curve is dominated by low-amplitude semi-regular pulsations, but no periodic long-term signal is present.

4.6 355.39−02.63

This is an excellent example of an S-type symbiotic with a very rich, high-ionization emission-line spectrum with all features present that would be expected including Raman-scattered O VI 6825. The OGLE light curve is typical for an S-type, resembling closely e.g. 003.46−01.92, with semi-regular pulsations from the red giant and an orbital variation of 854.5 d.

4.7 356.04+03.20

The emission-line spectrum is consistent with a highly ionized S-type symbiotic such as CI Cyg (Kenyon et al. 1991) and AX Per (Mikołajewska & Kenyon 1992). The Raman-scattered O VI 6825 feature is weak but its presence is consistent with the detected [Fe VII] emission.

4.8 357.98+01.57

The emission-line spectrum of 357.98+01.57 is typical of an S-type symbiotic. There may be a very weak detection of O VI 6825, but without any [Fe VII] emission lines, its presence is unlikely. Strong TiO λ8432 in the IR part of the spectrum suggests that the spectral type is as late as indicated by the VO band, i.e. most likely M5-6, where the weakness of the TiO bands at shorter wavelengths is caused by the symbiotic nebular continuum veiling the M giant. The OGLE-IV light curve in Fig. C6 shows

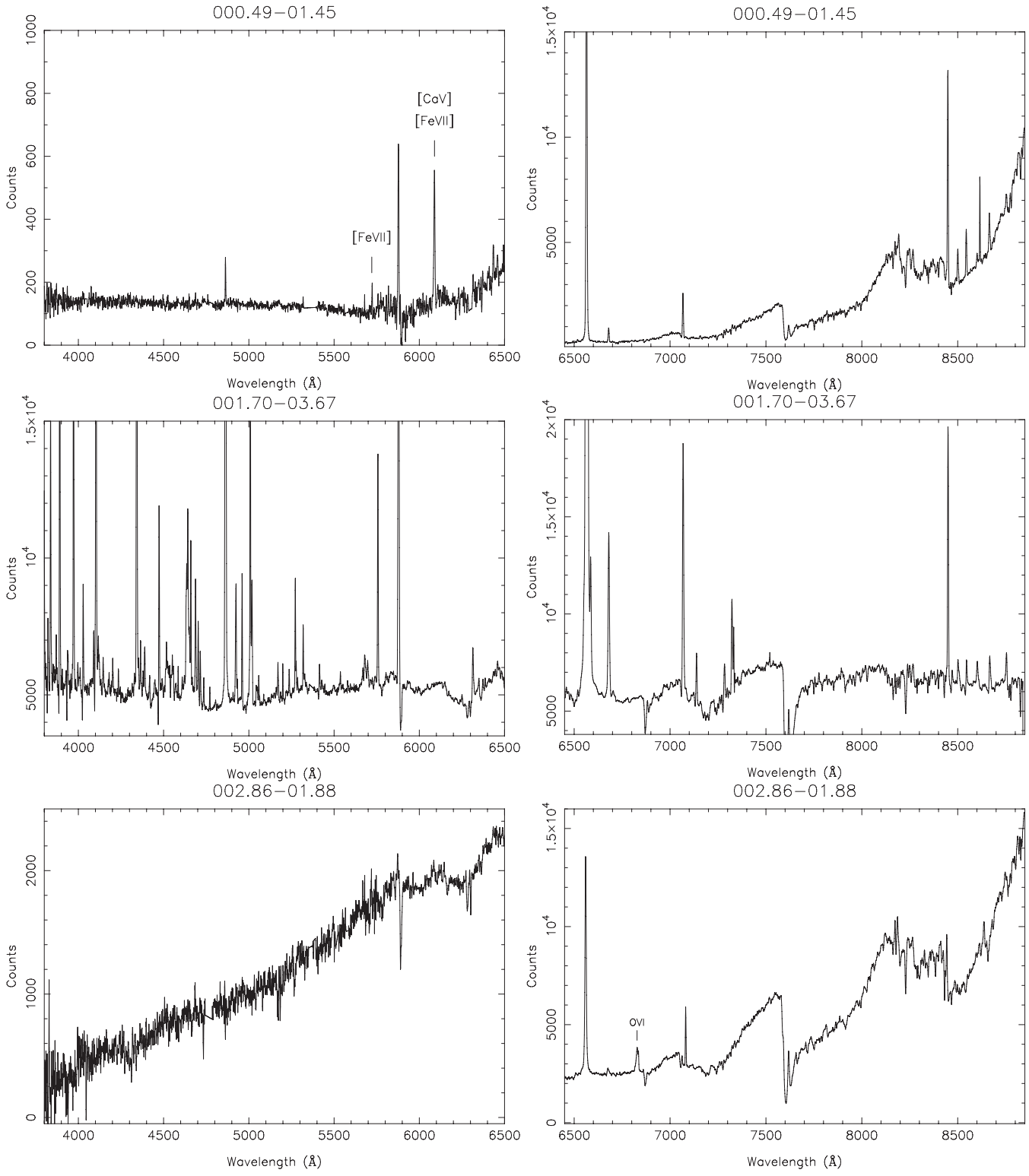

Figure 1. AAOmega spectra of new S-type symbiotic stars.

low-amplitude semi-regular pulsations of the red giant on top of longer term changes over 400–500 d, possibly due to orbital motion. The overall shape and time-scales are typical of S-type symbiotics, but it is too early to make any conclusions about an orbital period.

4.9 358.46+03.54

This is one of the brightest objects in our sample at $J = 9.19$ mag. As in 356.04+03.20, the rich emission-line spectrum is typical of a highly ionized symbiotic star. The O VI emission line appears to be

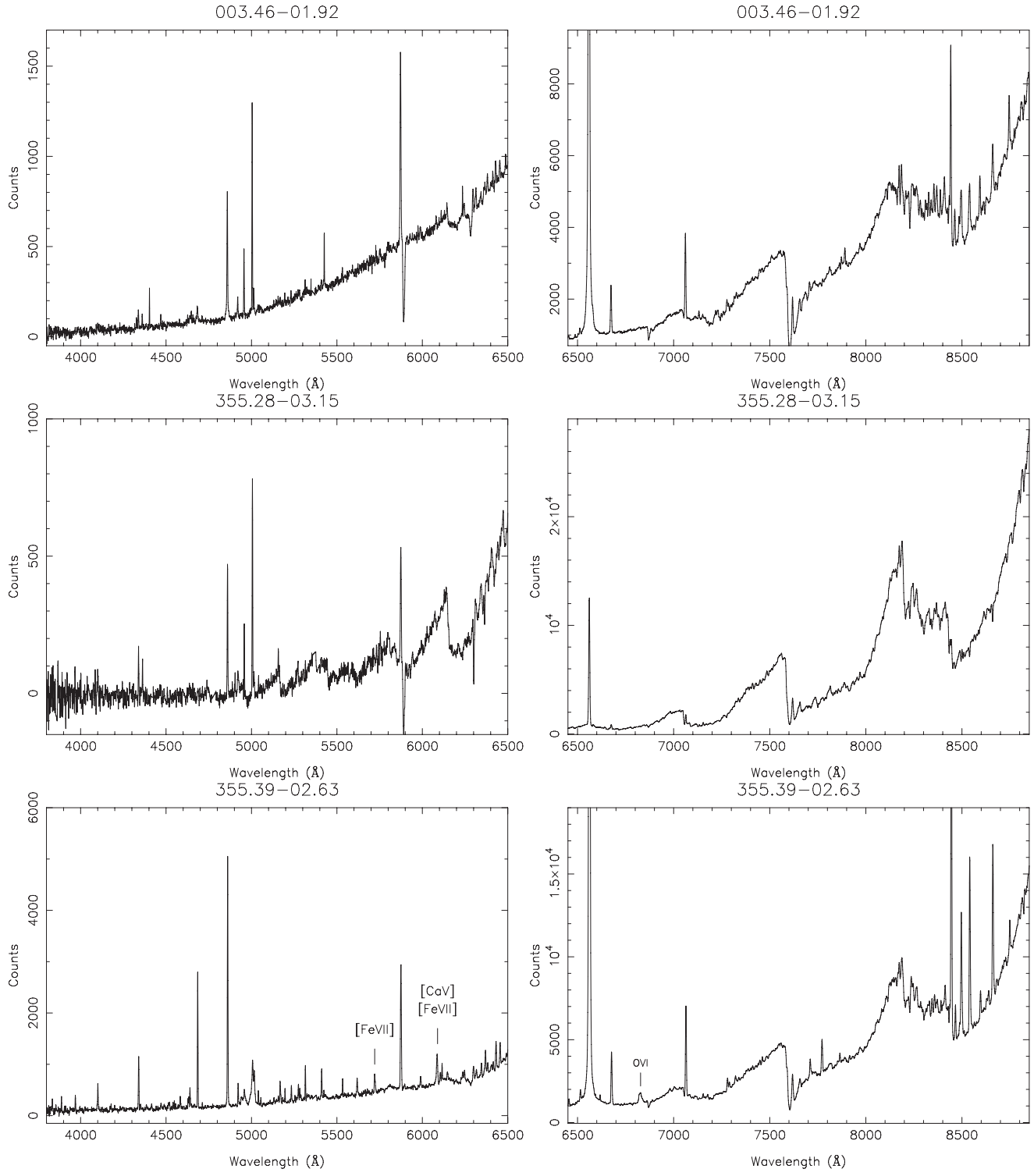

Figure 2. AAOmega spectra of new S-type symbiotic stars (continuation of Fig. 1).

blended with a nebular emission line, most likely [Kr III] λ6827 as seen in NGC 7027 (Zhang et al. 2005).

4.10 NSV 22840

NSV 22840 is a little studied variable star which Terzan & Gosset (1991) found to vary from $R = 17.7$ to 16.5 mag. Kohoutek & Wehmeyer (2003) noted strong Hα emission and a faint visible red continuum in their objective prism survey. The AAOmega spectrum proves its S-type symbiotic nature, and the OGLE-IV light curve shows what may be an eclipse in addition to semi-regular pulsations.

4.11 PHR 1757−2718

Listed as a possible PN by Parker et al. (2006) based on weak Hα in their published spectrum. In Table 8, we estimated a spectral type of

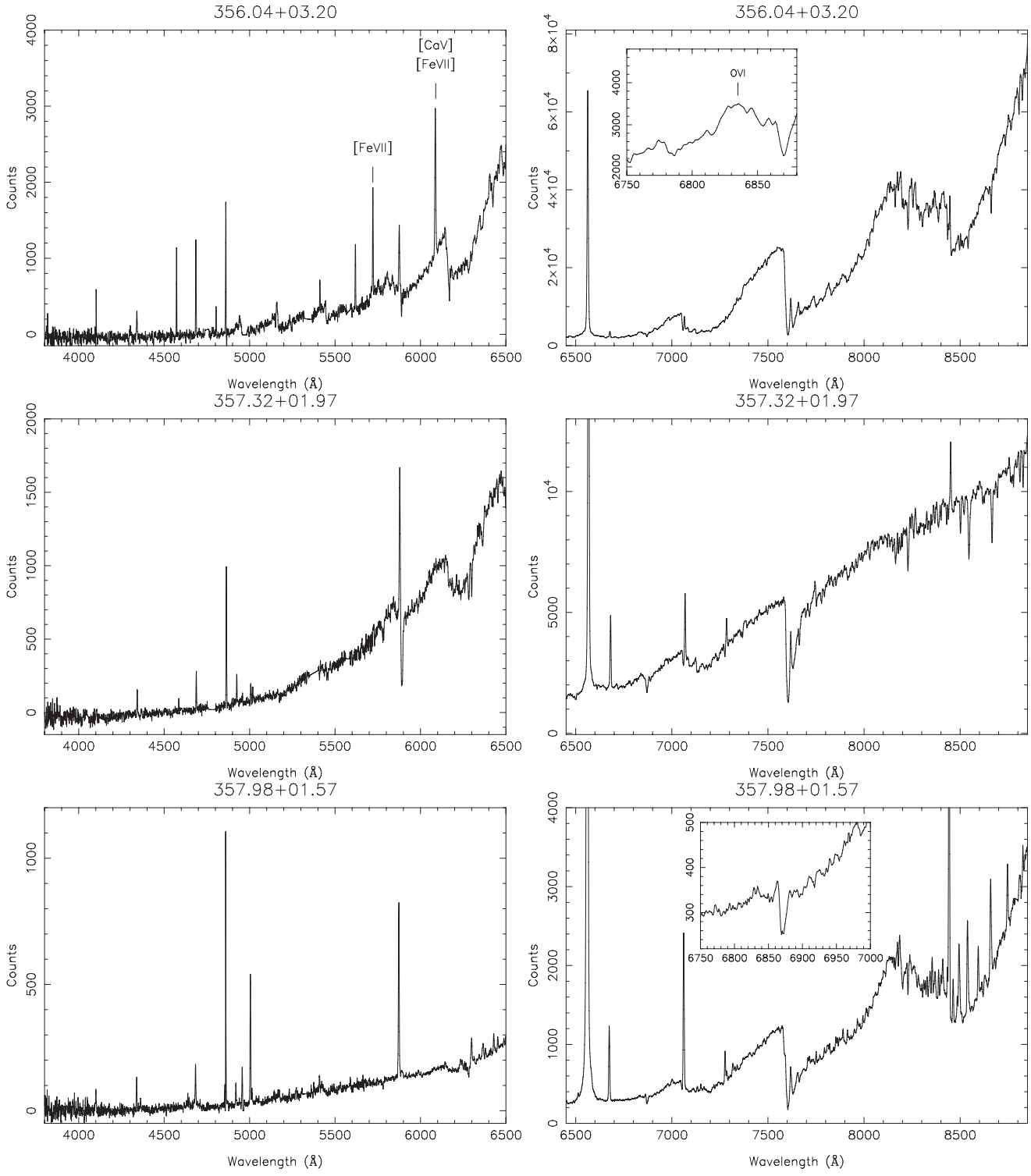

Figure 3. AAOmega spectra of new S-type symbiotic stars (continuation of Fig. 2).

M1-4 for the red giant; however, as in the case of 357.98+01.57, we suspect that the symbiotic nebular continuum is masking the TiO bands, suggesting a later spectral type of M5-6. The emission-line spectrum is typical for a highly ionized S-type symbiotic. Although the Raman-scattered O VI 6825 feature is very weak, its presence is probably real as there is also [Fe VII] emission. The OGLE-IV light curve shows long-term changes over 500–600 d that are most likely due to orbital motion. Continued photometric monitoring is necessary to confirm our preliminary orbital period of 585 d (see Fig. C7).

5 NEW D-TYPE SYMBIOTIC STARS

Figs 6 and 7 present the spectra of the new D-type symbiotic systems (except for JaSt2-6).

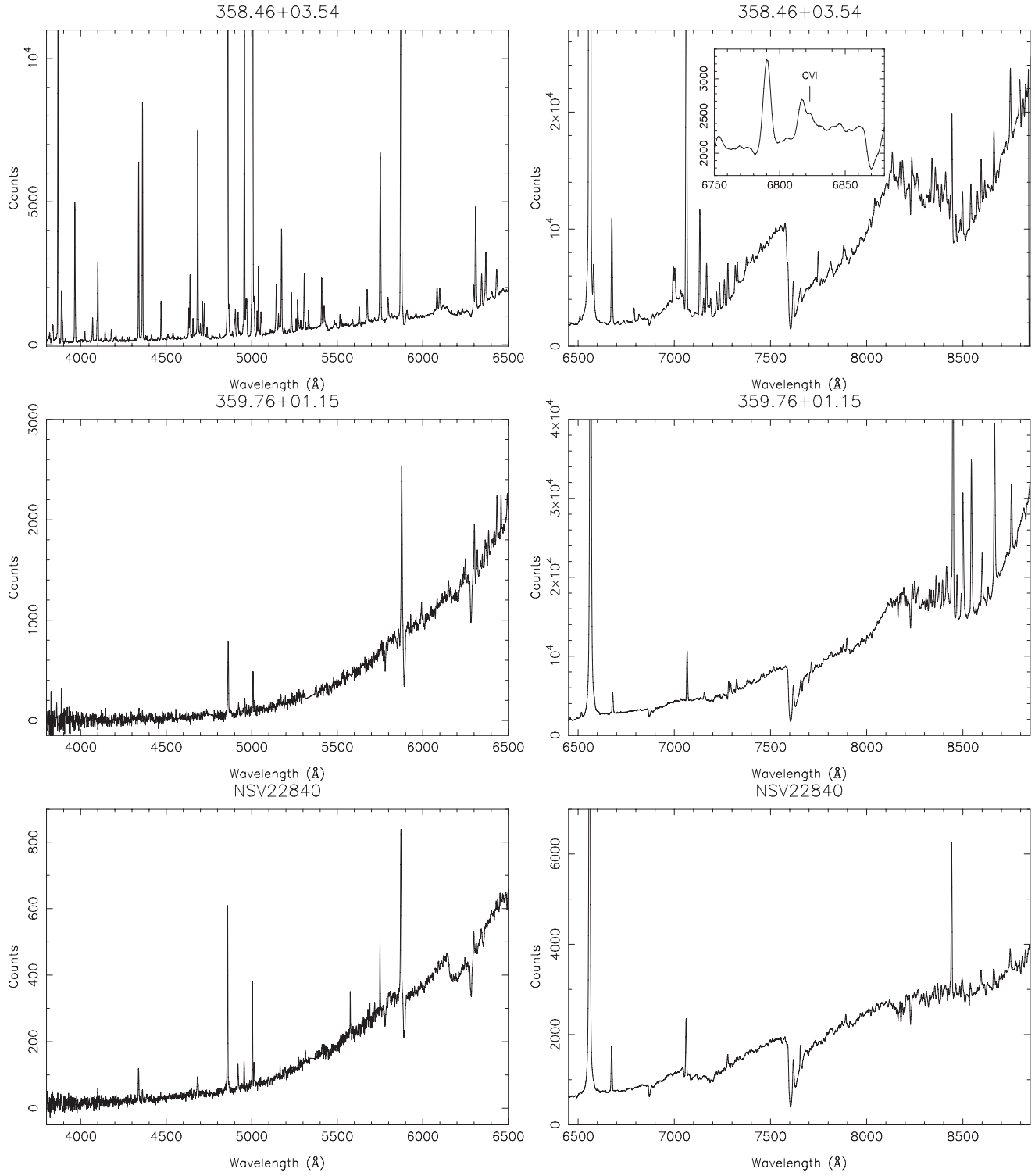

Figure 4. AAOmega spectra of new S-type symbiotic stars (continuation of Fig. 3).

5.1 354.98−02.87

This object shows a typical D-type emission-line spectrum complete with a weak detection of the Raman-scattered O VI 6825 feature. The very red 2MASS colours agree well with the known symbiotic Miras. The OGLE-IV light curve (Fig. C6) is the redder of two sources in Fig. D1, the one with $V - I = 1.59$ (slightly to NE) compared to $V - I = 0.281$ (slightly to SW). As would be expected for Miras embedded in their dust shell, the OGLE light curve detects only small variations and the Mira is not observed in the AAOmega spectrum.

5.2 H1-45

The AAOmega spectrum of H1-45 reveals strong emission lines typical of D-type symbiotic stars on top of a red continuum with

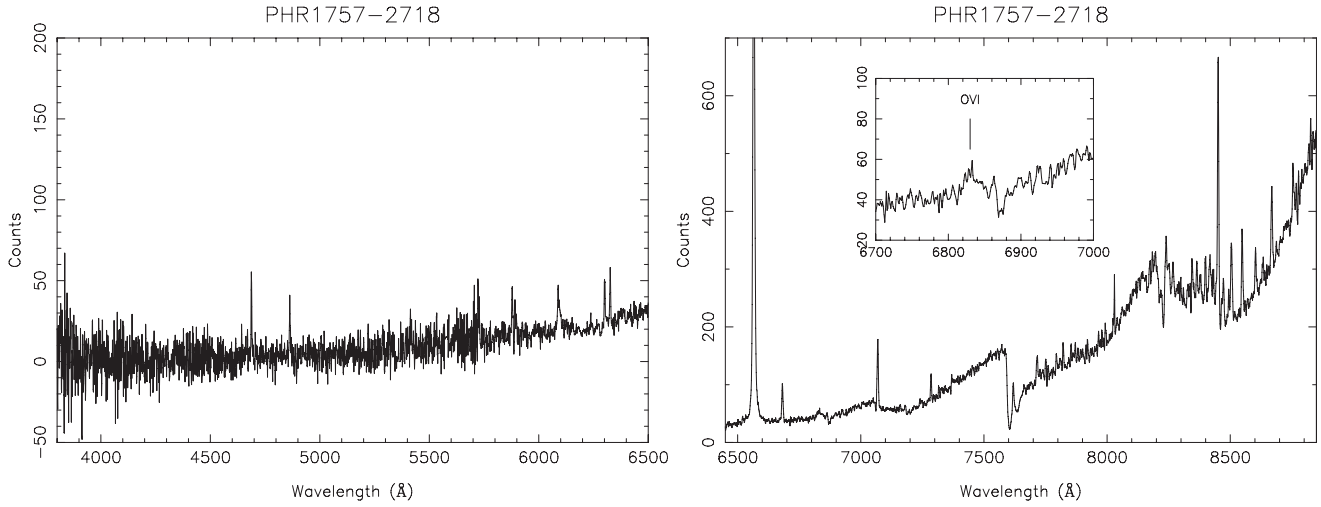

Figure 5. AAOmega spectra of new S-type symbiotic stars (continuation of Fig. 4).

strong CN bands and strong Ba II λλ 4554, 4934 and 6495 absorption lines. These properties are characteristic of a cool carbon star enhanced in s-process elements for which we assign a tentative spectral type of C4-C7 according to the Richer (1971) classification scheme. Furthermore, H1-45 is remarkable because of the 408.6 d pulsation period uncovered by the OGLE light curve, making H1-45 only the fourth known Galactic carbon-rich symbiotic Mira and the first luminous carbon star with likely Galactic bulge membership (Section 11.3). The three other Galactic systems known are SS38 and AS 210, with pulsation periods of 463 and 423 d, respectively (Gromadzki et al. 2009), and IPHAS J205836.43+503307.2, which is variable but does not yet have a determined pulsation period (Corradi et al. 2011). Another carbon-rich symbiotic in our sample may be ShWi5 (Section 6.1). There may also be some evidence for a dust obscuration event at the start of the OGLE light curve.

We can estimate the distance to H1-45 using the period–luminosity relationship for carbon Miras (Whitelock, Feast & van Leeuwen 2008). The 2MASS observations were taken at a pulsation phase of ∼0.79, implying that the observed K_s magnitude and colours may differ by ∼0.15 mag from their average values. The pulsation period of 408.6 d corresponds to an absolute magnitude of $M_K = -8.06 \pm 0.12$ (Whitelock et al. 2008), which when combined with the corrected 2MASS photometry results in $A_K = 0.78 \pm 0.2$ mag and $K_0 = 5.90 \pm 0.35$ mag. This results in a distance of $d = 6.2 \pm 1.4$ kpc suggesting either an intervening Galactic disc or near-side Galactic bulge membership. We discuss this crucial point further in Section 11.3.

H1-45 was also observed by the deep Hα, Sloan r' and i' imaging survey taken with the CTIO Blanco MOSAIC II instrument (Jonker et al. 2011). We retrieved these images from the NOAO archive[7] and created a quotient image Hα/r' to search for an extended Hα nebula. Despite the inner core (2–3 arcsec) being saturated in both Hα and r' images, the image quality is sufficient to rule out the presence of a larger extended nebula, in contrast to IPHAS J205836.43+503307.2 which appears to have a nebula (Corradi et al. 2011).

[7] http://portal-nvo.noao.edu

5.3 Hen2-375

The SAAO 1.9 m spectrum clearly proves Hen2-375 to be a D-type symbiotic star with both O VI Raman features detected amongst a rich emission-line spectrum. A giant companion is not detected in our spectroscopy, and we found no photometric variations in the ASAS light curve (Pojmanski 2002). In the colour-composite image of Hen2-375 made from SSS I_N (red), R_F (green) and B_J (blue) images (Hambly et al. 2001), we noticed an extended blue nebula (Fig. D3). To check whether this was a photographic flaw or not, we performed imaging in a variety of filters on the SAAO 1.0 m telescope. The STE4 SAAO CCD was used with 2 × 2 binning to give a pixel scale of 0.62 arcsec pixel^{-1}. Fig. 8 shows the nebulosity that was strongest in the [O III] filter ($\lambda_{cen} = 503.2$ nm, FWHM = 21 nm). Only a marginal detection in an Hα filter was recorded, consistent with previous findings that bipolar nebulae around symbiotic stars are very strong in [O III] emission (e.g. Solf 1984). Balmer line emission in such systems is strongly dependent on the density contrast of the nebula which in the polar direction is an order of magnitude less than in the orbital plane. The bipolar nebula measures 48 arcsec tip to tip and appears to be point symmetric (i.e. *S*-shaped). The SAAO 1.9 m spectrum was oriented at PA = 90°; however, it does not show any velocity structure in the extended [O III] emission. No spatially resolved [N II] emission lines from the nebula were detected in our spectrum, making it rather unusual amongst symbiotic nebulae that often show strong [N II] emission (e.g. Solf 1984). A Balmer decrement of Hα/H$\beta = 4.1$ was measured from the shorter exposures which corresponds to $E(B - V) = 0.33$ mag under Case B nebular conditions. This is a reasonable assumption since the line emission regions of D-types are usually located outside the thick dust shell and are only affected by interstellar reddening (e.g. Mikołajewska et al. 1997, 1999).

5.4 JaSt2-6

A pulsation period of 599.3 d was measured from OGLE-II data by Matsunaga, Fukushi & Nakada (2005). With now more OGLE observations, we have measured a similar 605.4 d. Surrounding the object is resolved Hα nebulosity, explaining its inclusion in the PN catalogue of Jacoby & Van de Steene (2004). Even though we lack deep spectroscopy of this system, these two facts combined

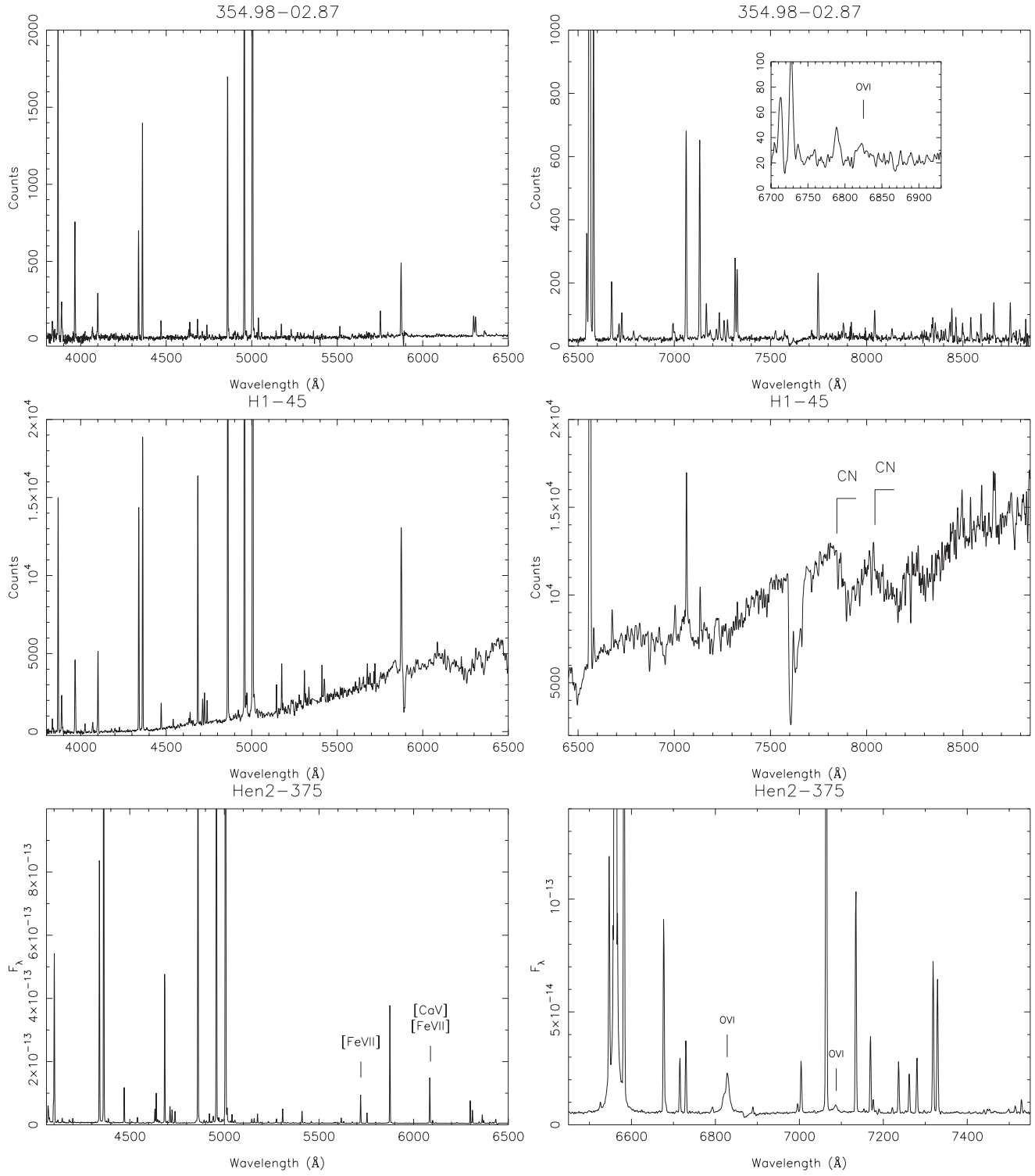

Figure 6. AAOmega spectra of new D-type symbiotic stars.

allow us to confidently classify JaSt2-6 as a symbiotic Mira. It is also detected by the *ROSAT* All-Sky Survey Faint Source Catalogue (see Voges et al. 2000; Section 11.2).

5.5 JaSt79

This was discovered by Van de Steene & Jacoby (2001) who remarked JaSt79 as a point source and also studied by Jacoby & Van de Steene (2004). The OGLE light curve shows a large *I*-band amplitude (>2 mag) and a period of 424.8 d, which when combined with the rich emission-line spectrum taken by 2dF/AAOmega clearly classifies JaSt79 as a symbiotic Mira. The Mira is detected in the AAOmega spectrum and does not appear to be carbon rich. We estimate a late M type based on the very strong TiO 8432 band, but the precise spectral type of the Mira is difficult to quantify because of the emission lines. As done for H1-45, we can also estimate the

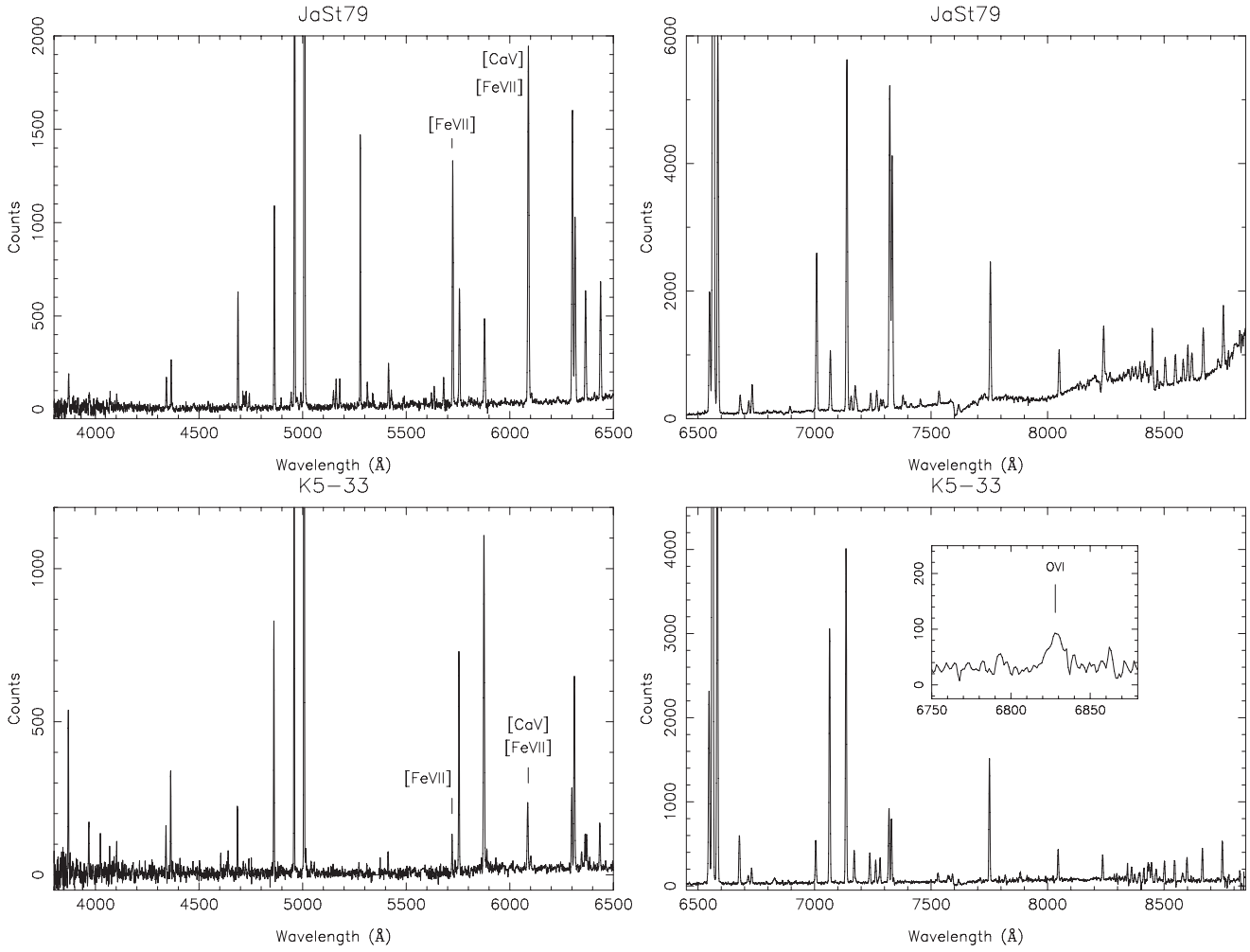

Figure 7. AAOmega spectra of new D-type symbiotic stars (continuation of Fig. 6).

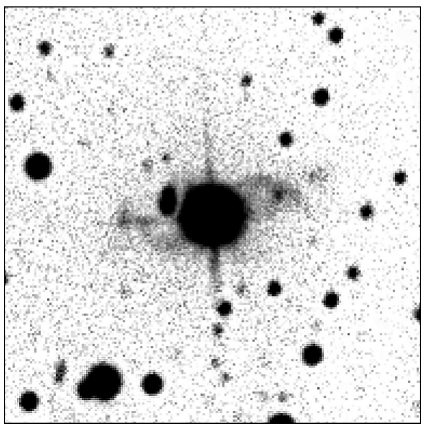

Figure 8. SAAO 1.0 m [O III] image of Hen2-375 with an unsharp mask applied. The image is 120 × 120 arcsec^2 with north up and east to left. The vertically elongated source NE of Hen2-375 is a filter artefact.

distance to JaSt79 using the period–luminosity relation for Galactic O-rich Miras (Whitelock et al. 2008). The 424.8 d period corresponds to $M_K = -8.12 \pm 0.12$ mag and the 2MASS photometry was taken at a pulsation phase of ∼0.36, requiring a correction of ∼0.15 mag to the K_s magnitude and colours. This yields $A_K = 1.1 \pm 0.2$ mag and $K_0 = 6.00 \pm 0.35$ mag, to give a distance of 6.7 ± 1.6 kpc. Slower variations in the OGLE light curve are probably due to dust obscuration (see e.g. Gromadzki et al. 2009) and JaSt79 may also be an X-ray source (see Hong et al. 2009; Section 11.2).

5.6 K5-33

This is the PN candidate PBOZ10 (Pottasch et al. 1988) and later rediscovered by Kohoutek (2002) as K5-33. It is however a clear D-type symbiotic with the Raman-scattered O VI 6825 feature detected and a typical D-type emission-line pattern. As in 354.98−02.87, the OGLE-IV light curve (Fig. C7) shows minimal variability, consistent with the D-type classification having an obscured Mira. The source identified in the OGLE image (Fig. D2) is the redder of the two in $V - I$.

6 NEW D′-TYPE SYMBIOTIC STARS

6.1 ShWi5

Discovered by Shaw & Wirth (1985), ShWi5 shows a rich emission-line spectrum on top of a red stellar continuum (Fig. 9). The 2MASS colours are consistent with a D′-type symbiotic, and this classification is supported by the warm carbon-rich giant detected in the AAOmega spectrum (equivalent to a late G-type). There are no

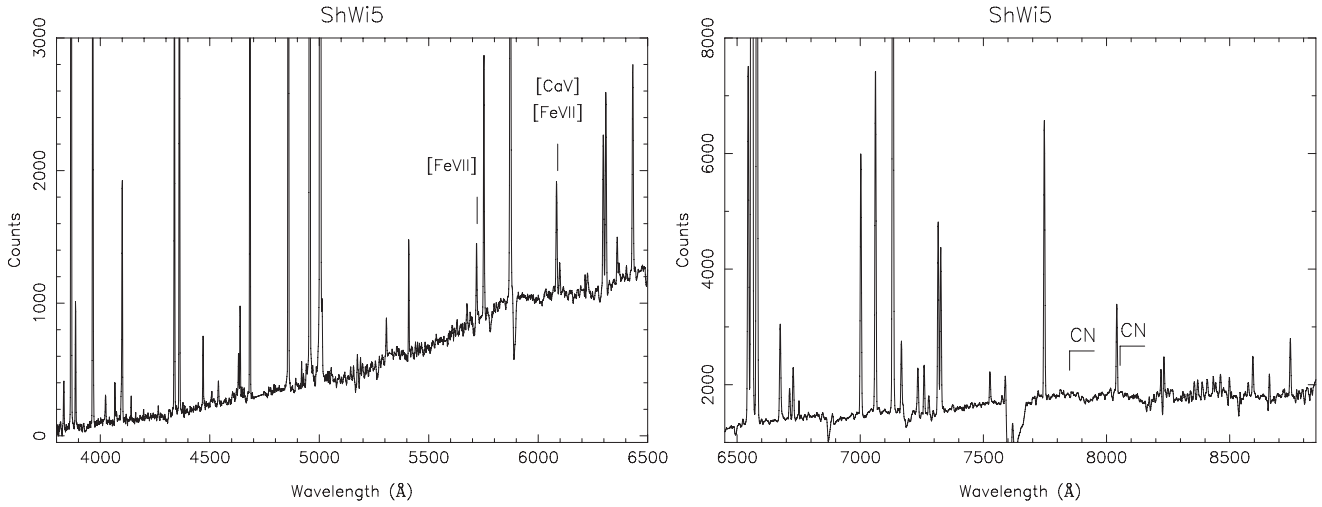

Figure 9. AAOmega spectrum of the new D′-type symbiotic star ShWi5.

TiO bands, but the CH band and weak CN bands are present, typical of other D′-types (Mürset & Schmid 1999) that often have solar metallicities and are overabundant in s-process elements (e.g. Pereira, Smith & Cunha 2005, and references therein). The continuum is complemented by [Fe VII] emission and an emission-line pattern typical of D′-type symbiotics. The light curve is relatively flat as is the case for most D′-type symbiotics (Gromadzki et al., in preparation); however, there may be some low-amplitude variability that could be ascribed to orbital motion.

7 POSSIBLE S-TYPE SYMBIOTIC STARS

The spectra of possible S-types are presented in Figs B1 and B2.

7.1 PPA 1752−3542

The spectrum published online by Parker et al. (2006) displays [O III] λ4363/Hγ > 1, Hα, Hβ and [O III] $\lambda\lambda$5007, 4959. Also present in the spectrum is an unrelated nearby late-type star that falls in the large 6.7 arcsec 6dF fibre diameter. The OGLE light curve resembles an S-type symbiotic star, but the system is too faint to be detected in 2MASS. Given the lack of better observations we leave this as a probable system that requires more observations to check our suspected S-type classification.

8 POSSIBLE D-TYPE SYMBIOTIC STARS

The spectra of possible D-types are presented in Figs B3–B5.

8.1 357.12+01.66 and PHR 1751−3349

Both objects have NIR colours consistent with D-type symbiotics; however, they lack the high-ionization emission lines that would be required for a definite symbiotic star status. We note that two well-studied symbiotic novae, RX Pup and V407 Cyg (Mikołajewska et al. 1999; Munari et al. 2011; Shore et al. 2011, 2012), both associated with D-type symbiotics, only show high-ionization lines during their nova outburst. Otherwise their optical spectra only show low-ionization emission lines (e.g. H I, ionized metals) and they may mimic B[e] stars (e.g. Lamers et al. 1998). Spectra of PHR 1751−3349 were taken during the OGLE light-curve minimum, and the light curve shows a large-amplitude slow variation typical of some D-type symbiotic stars. PHR 1751−3349 also has a small bipolar nebula that measures 13.5 arcsec tip to tip (0.5 pc at 8 kpc).

8.2 Al2-B

The broad wings on the [O III] $\lambda\lambda$4959, 5007 and Hα emission lines are not physical and are caused by inter-fibre contamination by a brighter PN observed in an adjacent fibre on the spectrograph pseudo-slit. A weak stellar continuum is also imprinted on the spectrum by the adjacent spectrum. Fainter features are however real, e.g. the λ4363/Hγ ratio. The possible D-type classification is based mostly on the emission-line spectrum since the 2MASS detection is too faint to allow for a meaningful classification.

8.3 Al2-G

The AAOmega spectrum shows an emission-line pattern similar to a D-type symbiotic. The most notable features being [O III] λ4363 > Hγ and strong [Ar IV] and [Ar V] emission lines. There may be a possible detection of [Fe VII] emission lines, but this requires further confirmation. During the OGLE-IV light curve, Al2-G slowly brightened by ∼0.1 mag, consistent with a slowly variable D-type system, which is also hinted at by the weak red stellar continuum in the AAOmega spectrum. As for Al2-B, the source is at the limit of what 2MASS can detect, so the colours are not meaningful in this case.

8.4 M2-24

Zhang & Liu (2003) presented spectroscopy of this very red source ($J - K_s = 3.61$ mag) which resembles other D-types in our sample with a highly ionized emission-line spectrum. Some peculiar features were detected including a high [O III] λ4363/Hγ ratio and the presence of Mg II. The OGLE finder chart reveals a bipolar nebula, and although a slowly brightening trend is seen in the OGLE light curve, presumably due to dust, we lack evidence for a solid D-type classification.

8.5 PHR 1803−2746

The emission lines detected by AAOmega are typical of a D-type symbiotic star but the stellar component in the spectrum is spurious,

coming from the nearby unrelated star. The OGLE-III *I*-band image shows the fibre diameter which in typical seeing would bring in light from this star.

8.6 PPA 1746−3454

The OGLE light curve is similar to PHR 1751−3349 and resembles that of some D-type symbiotic stars. The red 2MASS colours and AAOmega spectrum also resemble D-type symbiotics, but we lack the critical features necessary to secure a D-type classification.

8.7 PPA 1807−3158

The shallow spectrum published online by Parker et al. (2006) shows Hα, [N II] $\lambda\lambda$6548, 6583 as well as weak He I λ6678, [O I] $\lambda\lambda$6300, 6363 and [S III] λ6312. The red 2MASS colours and OGLE light curve are typical of D-type symbiotics, but as in the case of PPA 1746−3454 we lack the critical features to secure a D-type classification.

9 PNe WITH HDCS

At least five objects in our sample demonstrate nuclei or 'cores' that have properties more consistent with a symbiotic star, i.e. [Fe VII]/[Ca V] emission lines (requiring a dense environment with a hot ionizing source) and/or emission lines indicating densities $n_e \gtrsim 10^6$–10^7 cm^{-3}, but crucially do not show any evidence for a red giant companion or the Raman-scattered O VI emission bands. It is expected that a high-mass-loss-rate wind from a red giant is necessary to create the high densities found in symbiotic stars, so it is surprising that no red giants are present. Another source of high-density material may be dust remaining from the asymptotic giant branch (AGB) phase of the WD. Except for M2-29 (that we previously studied in Miszalski et al. 2011a), these objects are discussed in the following subsections after we summarize the few extant examples known.

The first such example to be studied was the CS of the evolved PN EGB6 (Ellis, Grayson & Bond 1984; Liebert et al. 1989; Fulbright & Liebert 1993; Bond 2009; Su et al. 2011). Since then only a few other examples have been identified including M2-29 (Torres-Peimbert et al. 1997; Miszalski et al. 2011a), Abell 57 and PHR 1553−5738 (Miszalski et al. 2011d) and PHR 1641−5302 (Parker & Morgan 2003; Frew & Parker 2010). Such peculiar CSs of otherwise normal PNe are now referred to as EGB6-like (Frew & Parker 2010), though this may be a diverse group so in this work we call them HDC PNe. An excellent example of this diversity is Hen2-428 for which Rodríguez, Corradi & Mampaso (2001) found a dense core ($n_e > 10^{10}$ cm^{-3}), but which was subsequently found to be a double-degenerate close binary CS (possibly a contact binary) with an orbital period of 0.18 d (Santander-García et al. 2011).

Figs 10 and 11 present spectroscopy of the five HDC PNe in our sample. Members of this class are suspected to share a similar binary configuration to EGB6, i.e. to have an M dwarf surrounded by a dense emission nebula (Bond 2009) located in a wide orbit (∼100 au) around the WD. Improving our understanding of dust obscuration events in HDC PNe may help us understand the origin of long secondary periods in some AGB stars (see e.g. Nicholls et al. 2009).

A dust disc is also anticipated to be present but its exact location is not known (Su et al. 2011). The only other HDC PN to show evidence for a dust disc is M2-29 which experienced a remarkable dust obscuration event in its light curve (Hajduk, Zijlstra & Gesicki 2008; Gesicki et al. 2010; Miszalski et al. 2011a). Miszalski et al. (2011a) applied a simple R Coronae Borealis star model (Goeres & Sedlmayr 1992) to the M2-29 light curve to determine that the dust responsible for these events forms at ∼70 au from the WD. This separation is comparable to the distance of the M-dwarf companion from the WD in EGB6. One possible explanation is that there is a dust disc around the M-dwarf companion rather than around the WD (e.g. Su et al. 2011). Another possibility is that the dust, leftover from the AGB phase in a surrounding circumbinary disc, is formed under the disturbing influence (wake) of the M-dwarf companion. A similar pinwheel-like effect is seen in AGB stars with companions (Maercker et al. 2012) and massive Wolf–Rayet stars (e.g. Tuthill, Monnier & Danchi 1999).

9.1 K2-17

K2-17 is a bipolar PN measuring 35 × 44 arcsec across with lobes visible to the east and west (Fig. D3). It resembles somewhat Abell 57 which also has an HDC (Miszalski et al. 2011d) and NGC 2371-2. The CS shows a clear Hα excess in the SHS data and is located in the centre of an apparent torus which is brighter on the SE side. Fig. 11 shows the typical high-excitation PN nebular spectrum (He II λ4686/Hβ = 1.2) which has a Balmer decrement of Hα/Hβ = 4.15 corresponding to $E(B-V) = 0.50$ mag. The nucleus notably shows a blue continuum with an S/N of ∼35 at λ5500 Å and ∼45 at λ6800 Å, the Ca II triplet in emission ($n_e \gtrsim 10^{10}$ cm^{-3}), [Fe VII] λ5721 and [Ca V]/[Fe VII] λ6087, C IV $\lambda\lambda$5801, 5812 and [Ar V] $\lambda\lambda$6435, 7005. We note that the [Fe VII] emission is substantially weaker than seen in the symbiotic stars of our sample. The spectrum somewhat resembles that of Hen2-428 (Rodríguez et al. 2001); however, it is unlikely to be a close binary as unpublished *I*-band photometry with the SAAO 1.0 m telescope found minimal variability. The asymmetric bipolar morphology and unusual spectrum strongly suggest that a main-sequence companion in a wide orbit is present. The 2MASS colours are rather red, suggesting the presence of warm dust as in some other HDC PNe, but this requires confirmation as the detection is near the limit for 2MASS.

9.2 M2-11 and M3-38

Fig. 12 shows the highly collimated outflows of these similar PNe. Each shows [Fe VII] emission from their nuclei. The average [O III] λ4363/Hγ ratios of 0.67 ± 0.05 and 0.55 ± 0.07 for M2-11 and M3-38, respectively, were calculated from the 20 spectra in the mini-IFUs. The errors represent the standard deviation σ of all 20 measurements, and the maximum value in each case did not exceed 2σ, suggesting that there is no real variation over the nebula that could be attributed to a dense nucleus. The weak emission lines at $\lambda\lambda$5801, 5812 may be members of the Pfund He II series (rather than C IV), of which several lines are visible just to the red of these lines in each object. Unfortunately, neither object has OGLE photometry.

9.3 PHR 1806−2652

PHR 1806−2652 was observed in the same FLAMES field as M2-29 (see Miszalski et al. 2011a). The mini-IFU for PHR 1806−2652 was centred on $18^h\,06^m\,56\overset{s}{.}07 - 26^\circ\,52'\,53\overset{''}{.}4$ at a PA of $135\overset{\circ}{.}24$ (see Fig. D2) which includes a CS whose 2MASS and GLIMPSE magnitudes are recorded in Table A2. The OGLE *I*- and *V*-band images show that the CS is slightly brighter in *V* and surrounded on either side by nebulosity in an *S*-shaped (bipolar) configuration. The nebula is visible in the SHS (Fig. D6), which also reveals an extra patch

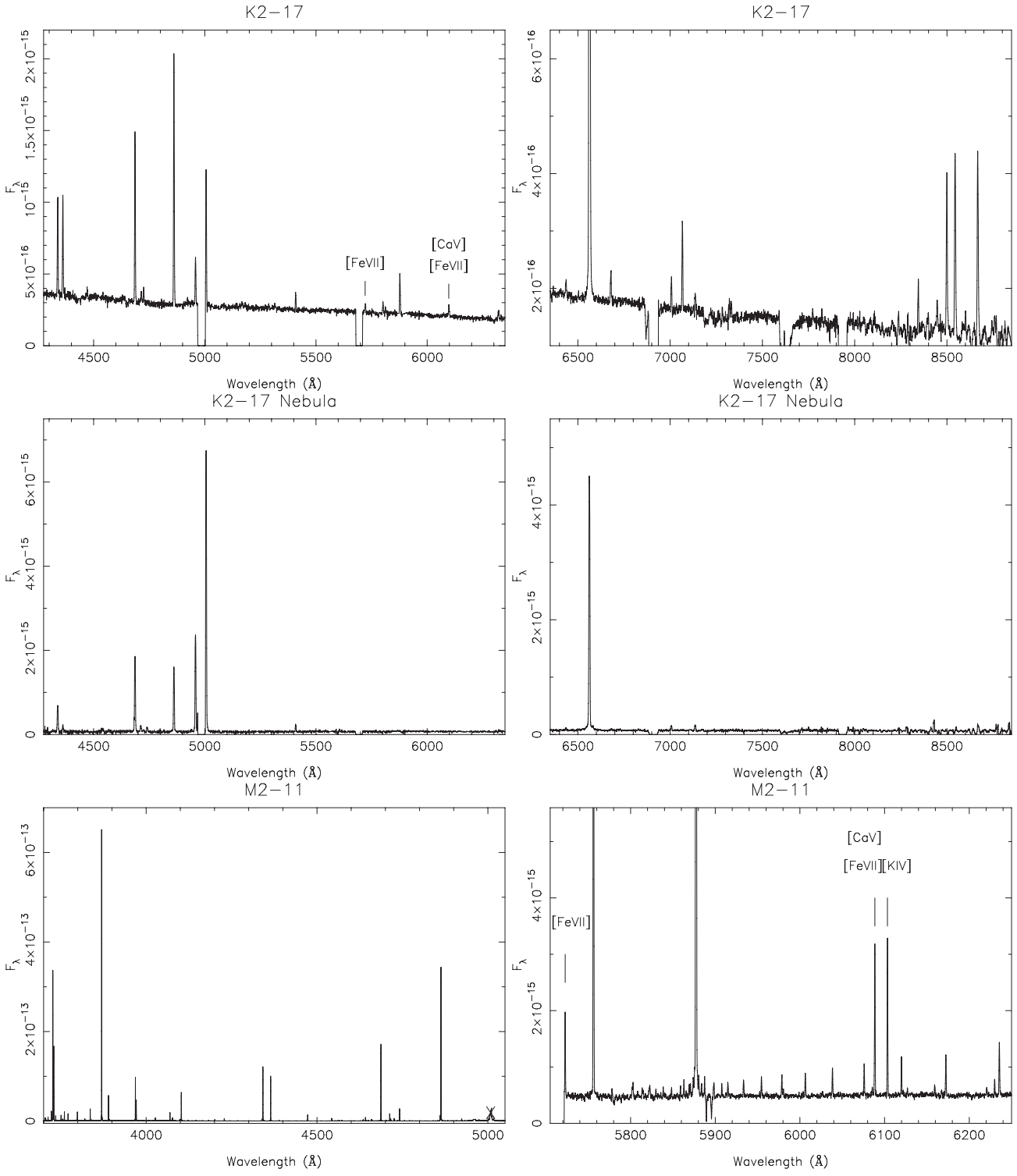

Figure 10. Spectra of HDC PNe.

of Hα nebulosity 34.1 arcsec to the SW which may be related at a separation of 1.3 pc at 8 kpc. The nebular morphology resembles the unusual He-rich object IPHAS J195935.55+283830.3 (Corradi et al. 2010a).

The emission-line ratios of the nebula are consistent with a PN after averaging all fibres. On the other hand, the [Fe VII] λ5721 and [Fe VII]/[Ca V] λ6087 emission originate from the CS and are not typical of PNe. The radial velocities of the [Fe VII] emission lines match those of the He I λ5876 emission line from the nebula. The S/N is too low to tell if there is stellar [O III] λ4363 emission, but the CS shows slightly broader Hα emission and stronger He I emission lines. No features of a companion are found, although we note that the apparent G band in Fig. 11 is spurious, originating from the integrated background light of the Galactic bulge. We estimated the reddening of $E(B-V) = 1.0$ mag from an average of estimates made from AAOmega and FLAMES spectra; the former estimate made

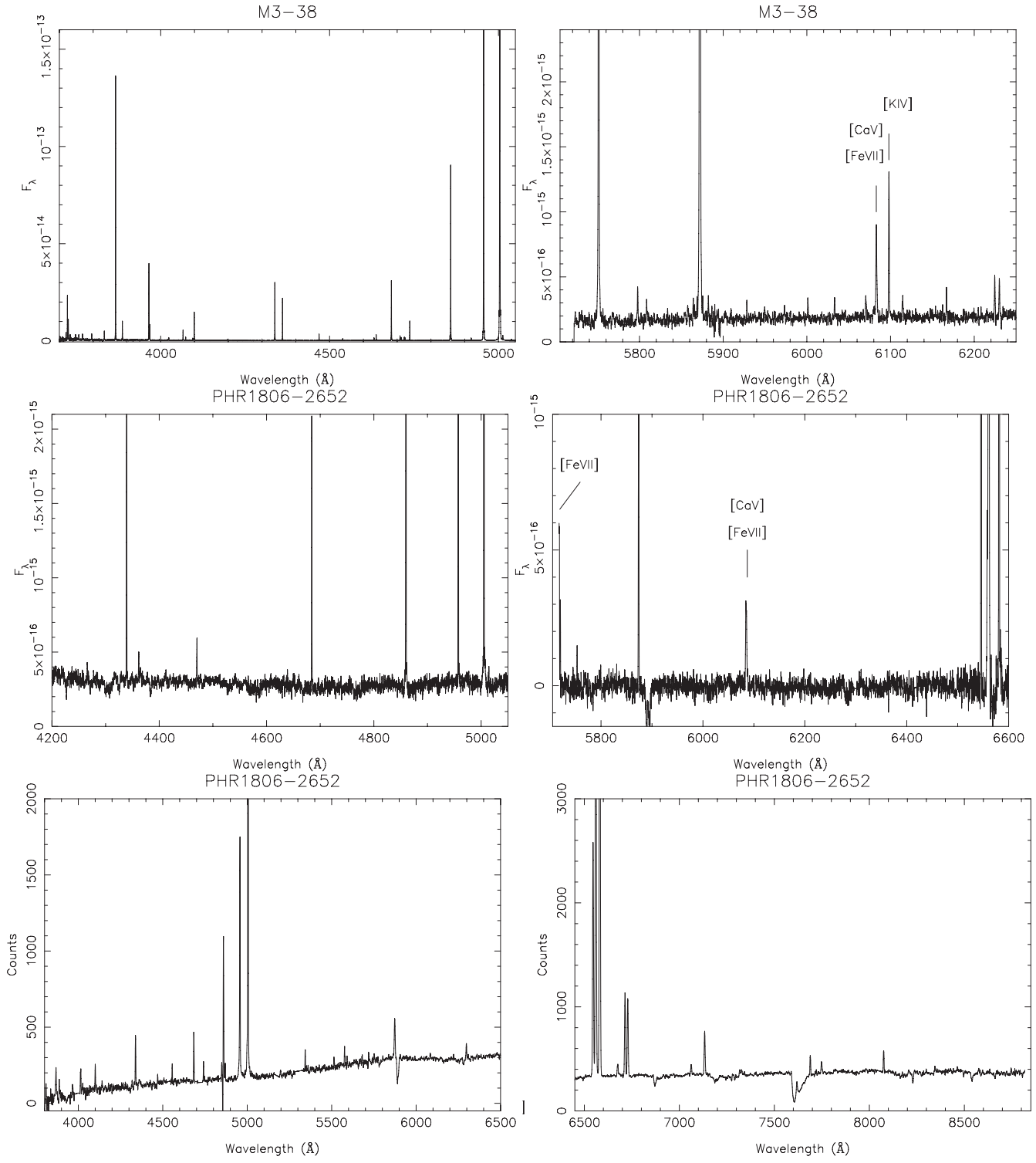

Figure 11. Spectra of HDC PNe (continuation of Fig. 10).

use of the [O III] λ5007/Hβ ratio from the FLAMES spectrum. This is rather high compared to $E(B-V) = 0.65$ mag of the very nearby M2-29 (Miszalski et al. 2011a), suggesting that the 0.3–0.5 mag uncertainty of this method is realistic and that the reddening may be closer to that of M2-29.

Fig. 13 presents the full OGLE *I*-band light curve of PHR 1806−2652. The light curve shows several dust obscuration events of up to ∼2.0 mag in depth that are considerably more frequent and irregularly spaced than in NGC 2346. A periodogram analysis of the light curve did not find any clear periodicity, consistent with the known pseudo-periodic nature of dust obscuration events (e.g. NGC 2346). Together with M2-29, PHR 1806−2652 suggests that dust obscuration events may be a common occurrence in the HDC PN class. Another PN to show dust obscuration events in our sample is MPA 1746−3412 which hosts a [WC10-11] CS (Section 10.3).

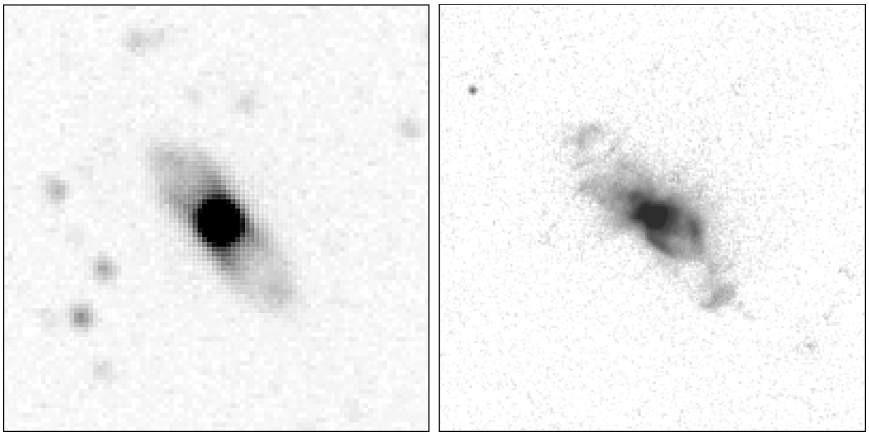

Figure 12. Images of the PNe M2-11 (left, ESO NTT/EMMI [O III] from programme 079.D-0764(B), 30 × 30 arcsec^2) and M3-38 (right, *HST* Wide Field Planetary Camera 2 *F*656*N*, 10 × 10 arcsec^2). Note the similarity in the highly collimated outflows surrounding both HDC PNe. North is up and east to left.

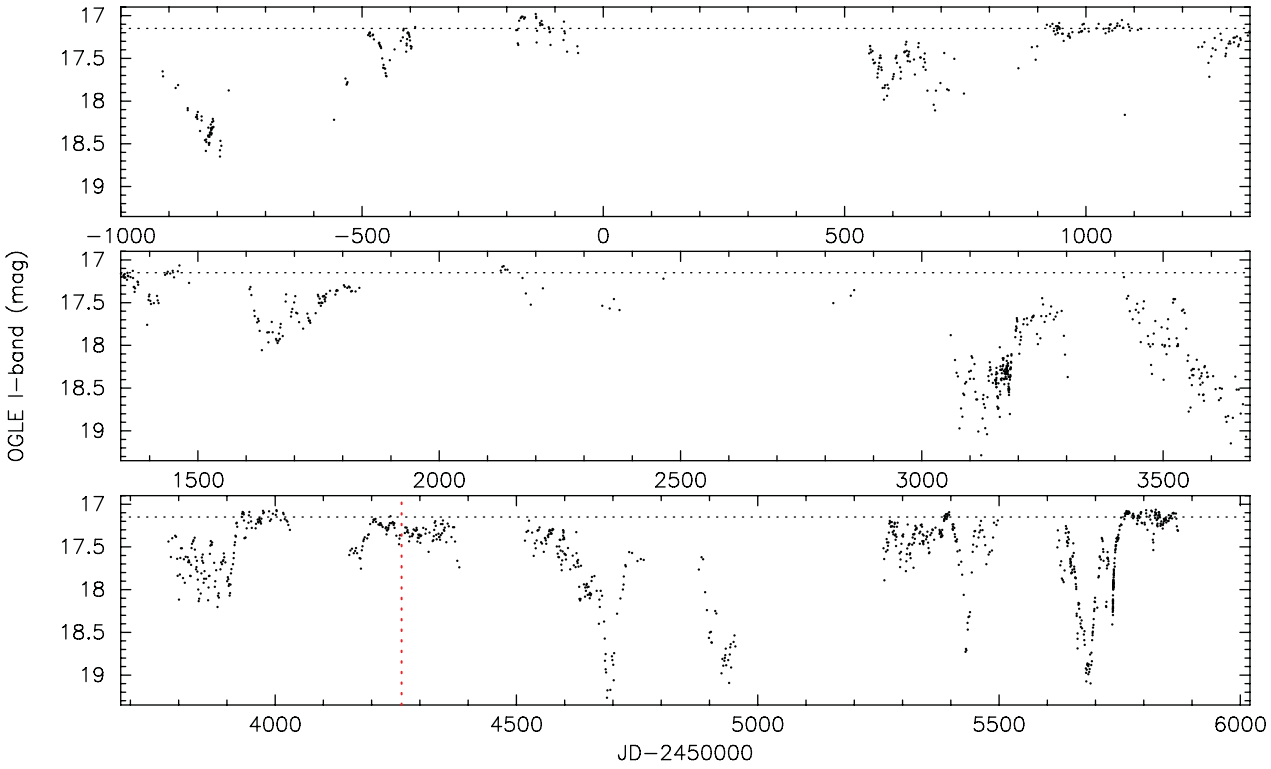

Figure 13. Full OGLE *I*-band light curve of the nucleus of PHR 1806−2652. The horizontal dotted line at $I = 17.15$ mag marks an arbitrary light maximum and the vertical dotted red line marks the epoch of the VLT FLAMES observations.

10 OTHER OBJECTS

10.1 Novae: 003.16−02.31 and V4579 Sgr

The strong He II, N III, [Fe VII] and C IV emission lines present in both spectra are typical of He/N-type classical novae in the nebular phase (e.g. Warner 2003). The MACHO light curves and, to a lesser extent, OGLE light curves show the decline of the novae over a span of 14.1 (003.16−02.31) and 18.7 (V4579 Sgr) yr. Fitting a line to the MACHO light curves we find decline rates of 1.2 × 10^{-3} mag d^{-1} (003.16−02.31) and 1.9 × 10^{-4} mag d^{-1} (V4579 Sgr). In the OGLE light curves, the corresponding rates are 9.6 × 10^{-5} and 2.8 × 10^{-5} mag d^{-1}, respectively. Discovery of V4579 Sgr is attributed to R. McNaught in 1986; however, we could not locate the corresponding IAU circular and it is listed as a slow nova in Samus et al. (2012). Woudt, Warner & Spark (2005) found 003.16−02.31 to have an eclipsing light curve with a period of 0.117 d and give further background information on the object. Some recent systematic studies of novae at similar stages in their evolution are Tappert et al. (2012) and Walter et al. (2012).

10.2 A B[e] star: PHR 1803−2748

Following Corradi et al. (2010a), the AAOmega spectrum of PHR 1803−2748 detects [Ni II] λλ6666, 7378 and 7412, which combined with the multiple [Fe II] lines and 2MASS colours indicative of hot dust classifies PHR 1803−2748 as a B[e] star (Lamers et al. 1998).

See also Miroshnichenko (2006) and the discussion by Frew & Parker (2010). A bipolar nebula is present and measures ∼18 arcsec tip to tip (0.7 pc at 8 kpc). Its presence suggests that PHR 1803−2748 may be a symbiotic B[e] star, but further observations are required to examine this possibility. The OGLE light curve shows slow changes similar to those seen in D-type symbiotic stars that are probably due to dust.

10.3 The [WC10-11] Wolf–Rayet CS of MPA 1746−3412

Fig. D1 identifies the object correctly which corresponds to object 57 from KW2003 (see later) which is clearly an Hα emission source (Fig. D3). The AAOmega spectrum is contaminated by the unrelated red giant (2MASS J17461818−3412370) immediately to the west of the object (Fig. 3). MPA 1746−3412 was included in table 1 of Miszalski et al. (2009a), but its peculiar spectrum is not a symbiotic star. It closely resembles other [WC10-11] Wolf–Rayet CSs of PNe (Leuenhagen, Hamann & Jeffery 1996), in particular Hen2-113 (Lagadec et al. 2006) and Hen3-1333 (Chesneau et al. 2006), but shows less stellar emission lines. The strongest emission lines of the Balmer series, [N II] and [S II], originate from the PN ionized by the cool [WC10-11] CS. The stellar spectrum is dominated by C II λ7235 and C III λ5696. Several other Galactic bulge PNe are known to show similar late-[WC] spectra (Górny et al. 2004, 2009) as well as one LMC PN (Miszalski et al. 2011b). Late-[WC] types were originally thought to be over-represented in the bulge (Górny et al. 2004), but this no longer seems to be the case following the discovery of several [WO]-type CSs by DePew et al. (2011).

Most interesting about MPA 1746−3412 is the OGLE light curve that shows a pseudo-periodic decline of 0.35 mag that repeats ∼1360 d and lasts for ∼950 d. This variability is most likely to be caused by dust obscuration events, as found in the [WC10] CS of Hen3-1333 (Pollacco et al. 1992; Jones et al. 1999; Cohen et al. 2002; Chesneau et al. 2006; Miszalski et al. 2011a). The recurrence time-scale between events in MPA 1746−3412 is comparable to those seen in Hen3-1333 (Miszalski et al. 2011a).

10.4 WN6 Wolf–Rayet stars: Th3-28 and 359.88−03.58

Acker & Stenholm (1990) reclassified Th3-28 to be a WR star and it is part of the van der Hucht (2001) catalogue as WR93a with a spectral type WN2.5-3. We reclassify the subtype as WN6 under the Smith, Shara & Moffat (1996) scheme since C IV λ5808 is only about 30 per cent greater than He I λ5876 in the peak/continuum ratio and N V is weak or absent.

359.88−03.58 was listed as an Hα emitter KW083 by Kohoutek & Wehmeyer (2003). The 2dF/AAOmega spectrum closely resembles Th3-28, and we also classify it as a WN6 star. The OGLE light curve is variable and shows smaller scale variations of ∼0.5 mag, probably pulsations, on top of a broader dip of ∼1 mag. A periodogram analysis found no periodicity in the variations. A dust obscuration event as in WC9 stars (e.g. Veen et al. 1998) is the most likely explanation for the observed variability and may indicate that a binary companion is present.

10.5 H2-32

The OGLE light curve shows a gradual rise of 0.3 mag and also shows small time-scale variability in very highly sampled parts of the OGLE-III and OGLE-IV observations. Fig. 14 shows one such part where an ∼5 d pseudo-periodic variation appears to be present, in addition to intra-day variability. The former may be an orbital period, while the latter is probably due to pulsations. These variations may be similar to those seen in Be stars (Porter & Rivinius 2003), but we find no clear signs of a B-type star in the low-resolution AAOmega spectrum. It may still be possible that this object is a PN with a relatively cool CS, passing through an instability strip, as seen in several PNe (Handler 2003). The 2MASS colours are not a helpful discriminant between PNe and Be stars, since both occupy a similar part in diagnostic diagrams (Corradi et al. 2008). At this stage we favour a possible Be star interpretation, based on the very unusual light curve which is atypical for PNe.

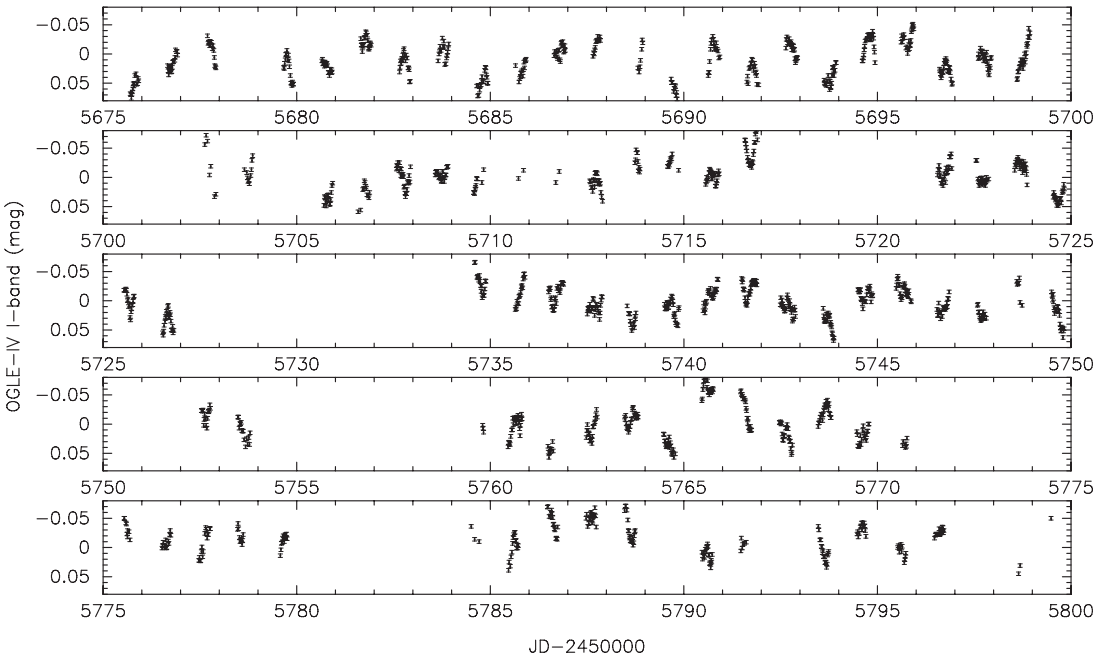

Figure 14. Part of the OGLE-IV *I*-band light curve of H2-32 showing intra-day variations about the mean.

10.6 PPA 1758−2628

The emission-line spectrum is rather ordinary besides the exceptionally strong He I emission lines. It is probably a highly reddened (compact) H II region. It is a source in NVSS (Condon et al. 1998), $F(1.4\,\mathrm{GHz}) = 13.7 \pm 0.6$ mJy, and is very bright in GLIMPSE, $F(8\,\mu\mathrm{m}) = (1.148 \pm 0.015) \times 10^3$ mJy. The 8 μm/NVSS flux ratio, a diagnostic developed for distinguishing PNe from H II regions (Cohen et al. 2007), has a very high value of 84, in the ultracompact H II region regime of Cohen et al. (2011). This classification is consistent with the emission-line spectrum that has unusually strong He I emission lines for a PN relative to other emission lines. This object is also listed as a radio compact H II region in Giveon et al. (2005).

10.7 Sa3-104

The OGLE-II and OGLE-III light curves both show a strong spurious periodicity of exactly 1 yr, most probably due to a non-stellar point spread function. Similar systematic effects were seen in other objects studied by Miszalski et al. (2009a). The periodicity does not appear in the higher quality OGLE-IV data. On the other hand, it is an interesting possibility that the slow decline may represent a real secular change, but we cannot prove this one way or the other. The AAOmega spectrum presents a low-excitation nebula with log (Hα/[N II]) = 0.35 and log (Hα/[S II]) = 1.91 consistent with Galactic PNe (Frew & Parker 2010). A weak stellar continuum shows absorption features of Ca II H&K and relatively broad Hγ and Hβ in absorption. These characteristics on their own are not remarkable, but we include it in our study because of its red appearance in the 2MASS colour-composite image and especially because of its exceptional brightness in GLIMPSE ([8.0] = 5.05 mag). As such the source may be a reddened H II region or possibly a Be star (Porter & Rivinius 2003). The non-detection of this source in the NVSS (Condon et al. 1998) with the bright GLIMPSE 8.0 μm flux seems to be consistent with this interpretation according to the MIR/radio ratio diagnostic (Cohen et al. 2007, 2011).

11 DISCUSSION

11.1 Completeness and depth

The completeness of the method used to select Hα emission-line candidates (Section 2) is best judged against lists of similar objects. We recovered 11/13 catalogued symbiotic stars coinciding with our AAOmega fields (Belczyński et al. 2000). This is depicted graphically in Fig. 15. Only two of these were not observed, Bl3-14 and Th3-31; the former can be explained by an overlapping star in the optical that essentially removed the apparent excess (the excess is comparable to residuals around field stars), while the latter had

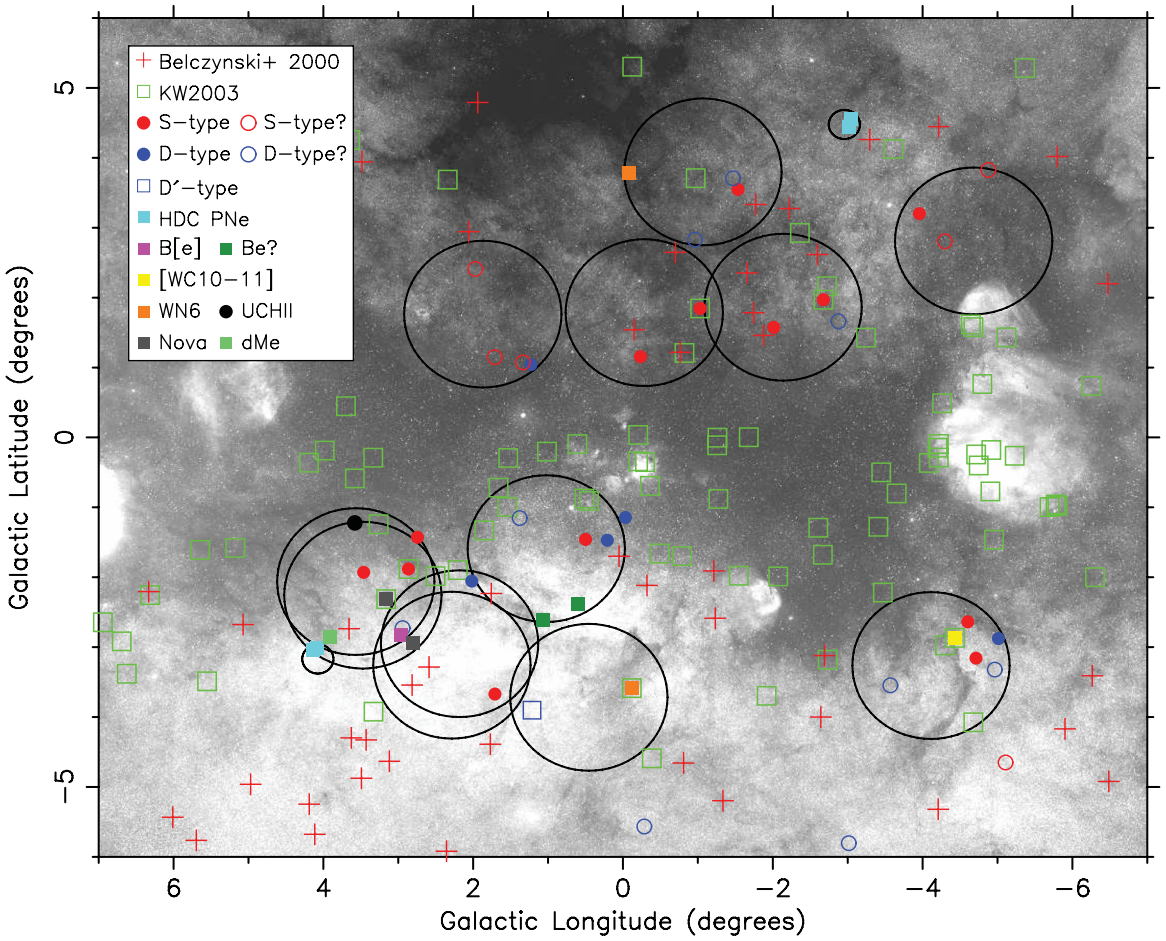

Figure 15. Mosaic of blocked-down SHS Hα fields overlaid with our sample, known symbiotics (Belczyński et al. 2000) and Hα emitters (KW2003). Fields observed with 2dF-AAOmega (Table 1) and FLAMES (Table 2) are shown by large and small circles, respectively. The D-type symbiotic star Hen2-375 and the HDC PN K2-17 are located outside this region at $(\ell, b) = (-22.7, -18.3)$ and $(-23.2, -07.2)$, respectively.

Table 13. The 17 Hα emission-line objects from table 1 of KW2003 that are located within our AAOmega fields.

Field	KW	Name	Type
N5	022	–	–
N2	023	–	–
N2	025	357.32+01.97	S
N3	037	NSV 22840	S
N3	042	–	–
S3	057	MPA 1746−3412	[WC10-11]
S3	059	–	–
S18	065	–	–
S18	066	–	–
S18	073	–	–
S18	075	–	–
S21	079	–	–
S21	081	–	–
S21	082	002.86−01.88	S
S22	083	359.88−03.58	WN6
S3	102	–	–
S21	105	003.16−02.31	Nova

no optical counterpart to a very red source visible in 2MASS ($J - K_s = 3.6$, 2MASS J173426666−2928029). AAOmega spectra of these known symbiotic stars will be studied elsewhere.

A more comparable sample of Hα emitters is those discovered by the objective prism survey of Kohoutek & Wehmeyer (2003, hereafter KW2003). Table 1 of KW2003 lists 98 new Hα emitters and 9 probable Hα emitters that are more numerous at lower latitudes ($|b| \lesssim 1^\circ$). These sources are included in Fig. 15. Table 13 delineates the subset of KW2003 sources located in our AAOmega fields and their observation status. Of the objects we missed, inspection of the SHS and SSS images found that both KW081 and KW022 are small, i.e. easily missed when viewing large areas, while only KW023 shows a modest Hα excess that might have been selected. The remainder show only weak Hα excesses that explain their exclusion from our AAOmega observations.

The completeness of our survey is therefore reasonably high, though it is difficult to quantify this further. For example, we identified Hα emitters that were not found by KW2003, and only the best candidates were selected in the densest fields (e.g. S18) where the Hα emitters were more numerous and it was more difficult to judge the level of Hα excess. Nevertheless, we are the first to systematically combine deep spectra and *I*-band light curves to discover new symbiotics, greatly enhancing the completeness of our survey over previous works. In the $\sim$35 deg^2 considered in our survey, we have more than doubled the number of confirmed symbiotics. Combining our new discoveries with Belczyński et al. (2000), we can also calculate an average symbiotic star surface density in northern ($b > 0^\circ$) and southern ($b < 0^\circ$) AAOmega fields based on five fields each of radius 1.°05. We found 0.9 ± 0.7 and 1.0 ± 0.4 deg^{-2} for confirmed symbiotics in northern and southern fields, respectively, where the errors represent the standard deviation of measurements from each of the five fields. If we include the possible symbiotic stars, these values are 1.3 ± 0.4 and 1.3 ± 0.6 deg^{-2}, respectively. This constitutes a first estimate of the surface density of symbiotic stars towards the Galactic bulge, which may in the future be compared with stellar population models that also take into account the complex interstellar extinction towards that bulge, to better constrain the total number of Galactic symbiotic stars (see e.g. Corradi et al. 2010a; Corradi 2012).

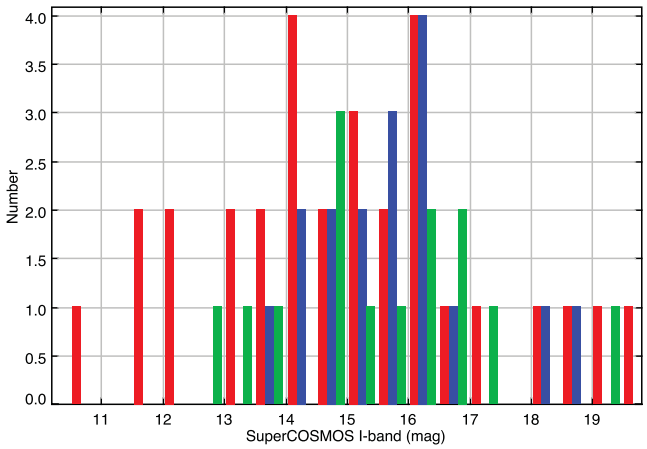

Figure 16. SSA *I*-band magnitude comparison between known symbiotics (red, Belczyński et al. 2000), our new symbiotics (blue, this work) and symbiotics discovered so far by IPHAS (green, Corradi 2012 and references therein). The bin size is 0.5 mag with each data series shown in three adjacent columns per bin.

A general comparison can also be made with other symbiotic stars to assess the depth of our survey. Modern CCD-based photometry is not generally available for the Galactic bulge at optical wavelengths, making a uniform comparison challenging. The depth of 2MASS is insufficient for the faintest objects in the NIR, while not all objects have OGLE-III *I*-band coverage. Uniform coverage is however available with digitized photographic all-sky survey catalogue photometry available online in the SuperCOSMOS Science Archive[8] (SSA; Hambly et al. 2004). Here we make use only of the *I*-band magnitudes since bluer filters are strongly influenced by reddening and strong Hα emission. A nearest-neighbour cross-match was performed with the SSA for our new symbiotic star sample (excluding Hen2-375), the known symbiotic stars (Belczyński et al. 2000) bounded by the Galactic coordinate range in Fig. 15 and the IPHAS-selected symbiotic stars (Corradi 2012). Fig. 16 displays the histogram of *I*-band magnitudes, and no attempt was made to correct the data for photometric variability. The data show our sample to fall towards the fainter end of the magnitude distribution of known symbiotics, suggesting that our improved survey techniques have allowed us to identify relatively fainter symbiotic stars than previous surveys. Our sample is however comparable to the symbiotics discovered by IPHAS that are located outside the Galactic bulge (Corradi 2012 and references therein).

11.2 X-ray properties

Symbiotic stars may also be detected at X-ray wavelengths due to a variety of emission mechanisms (e.g. Mürset, Wolff & Jordan 1997; Luna et al. 2012). Supersoft sources are an indication of massive WDs and are usually associated with low-metallicity environments (e.g. Kato et al. 2013). We searched for an overlap between our sample and the *Chandra* Galactic Bulge Survey X-ray catalogue of Jonker et al. (2011). The survey consists of a series of relatively shallow 2 ks pointings in which 10 sources overlap (000.49−01.45, 357.98+01.57, 359.76+01.15, JaSt2-6, JaSt79, NSV 22840, PHR 1757−2718, 001.33+01.07, 001.37−01.15 and 001.71+01.14). None, however, had a corresponding detection within 30 arcsec

[8] http://www-wfau.roe.ac.uk/ssa/

under the selection criteria applied by Jonker et al. (2011). Several long-period variables were identified by Udalski et al. (2012) to match with other sources catalogued by Jonker et al. (2011).

There are two objects that may have X-ray detections in other surveys. The *ROSAT* All-Sky Survey Faint Source Catalogue (Voges et al. 2000) detected a source, 1RXS J175001.8−293316, located 8.6 arcsec from JaSt2-6 with a count rate of 5×10^{-2} counts s^{-1} and positional error of 37.0 arcsec. Such a source would probably have been detected by Jonker et al. (2011), so this may be an indication of X-ray variability that needs further monitoring. Hong et al. (2009) obtained much deeper (100 ks) *Chandra* observations towards the bulge and catalogued an X-ray source (J175153.6−293054) 2.0 arcsec away from JaSt79 with a median energy of 1.127 keV and a 2σ positional error of 1.67 arcsec. While this detection seems reliable, it would be unusual given the relatively large distance (∼6.7 kpc) and high reddening [$E(B-V) \sim 2.5$ mag] to JaSt79. As we detect the Mira spectroscopically and its pulsations in the OGLE light curve, the bulk of the reddening must be interstellar and is likely to suppress such X-ray emission if it originated from JaSt79. Further dedicated observations are needed to confirm whether it is a true detection.

11.3 H1-45: the first probable Galactic bulge carbon Mira

A longstanding problem in stellar astrophysics is the lack of luminous carbon stars belonging to the Galactic bulge (e.g. Whitelock 1993; Whitelock et al. 1999; Ng 1999; Feast 2007; Wahlin et al. 2007). A small sample of intrinsically faint, relatively blue carbon stars has been documented (Azzopardi, Lequeux & Rebeirot 1985; Azzopardi et al. 1991; Westerlund et al. 1991; Alksnis et al. 2001), but none rival the luminosities of bona fide carbon stars found elsewhere and they may be the product of binary evolution (Whitelock et al. 1999). The luminosity of H1-45 is instead typical of carbon Miras ($M_K = -8.06 \pm 0.12$ mag) and its estimated period–luminosity relation distance of 6.2 ± 1.4 kpc places it within the reach of the Galactic Centre ($d \sim 8.0 \pm 0.5$ kpc; Matsunaga, Fukushi & Nakada 2013). At the short end of 4.8 kpc, its distance would be consistent with membership of the Galactic disc. While we cannot rule out disc membership, it seems more likely, however, that it belongs to the Galactic bulge. At the Galactic coordinates of H1-45, studies of red clump stars have shown that the inner Galactic bar extends nearer to us than at negative longitudes, in some cases reaching a distance of 6 kpc from the Sun (Stanek et al. 1997; Babusiaux & Gilmore 2005; Cabrera-Lavers et al. 2007; Rattenbury et al. 2007; Gonzalez et al. 2011). It is therefore possible that H1-45 is situated at the near end of the inner bar. One way to test this further would be to identify the source of the carbon enhancement in H1-45, whether it is intrinsic, produced by the visible carbon Mira, or extrinsic, produced by the AGB progenitor of the WD companion. If the Galactic bulge cannot produce carbon stars, as seems to be the case, then a Galactic disc membership would be more consistent with an intrinsic rather than extrinsic origin.

11.4 Tendencies amongst each symbiotic star type

The discoveries made in this paper reinforce the observed properties of each symbiotic star type and highlight the challenges in proving a symbiotic star classification. A telling statistic is the ratio of the number of S-types to D-types (S/D) in the new (S/D = 2.2) and possible (S/D = 0.7) samples. Clearly, the S-types are more straightforward to confirm, owing to the generally unobscured cool stellar photospheres of the donor being readily observable at optical wavelengths. The light curves of S-types in both our new and possible samples readily demonstrate semi-regular pulsations from the donor star, a trend also noticed in known S-type symbiotics (Gromadzki et al., in preparation).

At optical wavelengths D-types are considerably more difficult to confirm, owing to the presence of warm dust as seen in their NIR colours. In most cases, this dust forms an obscuring shell or cocoon around the Mira component, rendering the spectral signatures and pulsations of the Mira invisible at far-red and shorter wavelengths. This is best demonstrated by RX Pup, where the Mira pulsations are only seen at NIR wavelengths and its absorption spectrum has never been observed at optical wavelengths (Mikołajewska et al. 1999). Without these signatures at optical wavelengths, the D-types typically show their PN-like nebular spectra, originating near the relatively unobscured hot WD, and optical light curves that are either flat (e.g. 354.98−02.87 and K5-33) or only slowly variable due to dust obscuration (e.g. Al2-G, PPA 1746−3454, PHR 1751−3349 and PPA 1807−3158; see also Gromadzki et al. 2009). Pulsations from the Mira components in these D-type systems should be readily visible in NIR light curves, but these are not readily available. Nevertheless, we were fortunate that some systems are less reddened, allowing for their Mira pulsations to be detected, confirming them as D-type symbiotics (H1-45, JaSt2-6 and JaSt79).

12 CONCLUSIONS

We have conducted a survey of Hα emission-line stars towards the Galactic bulge covering ∼35 deg^2. Deep optical spectroscopy and *I*-band long-term light curves were presented for most of the sample, revealing 20 new and 15 possible symbiotic stars, as well as several other unusual emission-line stars. The novel incorporation of light curves has proven particularly effective in proving the symbiotic status of several objects whose classification may have remained ambiguous from optical spectroscopy alone.

The main conclusions are as follows.

(i) A total of 20 symbiotic stars were confirmed, consisting of 13 S-types, 6 D-types and 1 D′-type, of which 35 per cent show the Raman-scattered O VI features. Orbital periods were determined for five S-types and Mira pulsation periods for three D-types. Further study of a list of 15 possible symbiotics (six S-types and nine D-types), particularly at NIR wavelengths to search for Mira pulsations in the case of D-types, should allow for more symbiotics to be confirmed.

(ii) H1-45 was found to be a carbon symbiotic Mira and is only the fourth now known in the Galaxy. Using the Whitelock et al. (2008) period–luminosity relation, the carbon Mira pulsation period of 408.6 d corresponds to a distance of 6.2 ± 1.4 kpc and an absolute magnitude of $M_K = -8.06 \pm 0.12$ mag. If it belongs to the near side of the Galactic bulge, then it would be the first luminous carbon star identified in this environment, potentially offering a means to solve the longstanding missing Galactic bulge carbon star puzzle (e.g. Feast 2007). Further observations of H1-45 are essential to further refine the distance to this unique object and understand its origin in the context of carbon star formation as a function of environment (e.g. Nowotny et al. 2013). The D′-type symbiotic ShWi5 may also be carbon rich, but it requires further study.

(iii) Dust obscuration events were discovered in the CSs of PHR 1806−2652 and MPA 1746−3412, increasing the sample of PNe showing such behaviour to five PNe. The CS of PHR 1806−2652 exhibits [Fe VII] emission and belongs to the HDC PN family, i.e. it

has symbiotic-like characteristics, but these are thought to be associated with main-sequence companions and circumbinary dust discs. Three other HDC core PNe were also presented. MPA 1746−3412 has a [WC10-11] Wolf–Rayet CS and therefore strongly resembles the very similar Hen3-1333. A dust obscuration event was also noticed in the massive WN6 star 359.88−03.58, suggesting that it may be a binary system.

(iv) Comparison with other catalogues of Hα emitters (KW2003) and symbiotic stars (Belczyński et al. 2000) demonstrated the high completeness of our survey. The apparent surface density of all symbiotic stars in the $\sim$35 deg^2 of our survey amounts to $\sim$1.0–1.3 deg^{-2}. Much further work remains to create a complete consensus of Galactic bulge symbiotic stars in order to improve estimates of the total Galactic symbiotic star population (Corradi et al. 2010a; Corradi 2012).

ACKNOWLEDGEMENTS

This work benefited from the framework of the European Associated Laboratory 'Astrophysics Poland-France'. JM is supported by the Polish National Science Center grant number DEC-2011/01/B/ST9/06145. The OGLE project has received funding from the European Research Council under the European Community's Seventh Framework Programme (FP7/2007-2013)/ERC grant agreement No. 246678. We would like to thank the referee, Romano Corradi, for insightful comments that have helped improve some aspects of this paper.

We thank AAO staff for performing the AAOmega service observations and especially R.G. Sharp for taking additional observations. This work is partly based on observations made at the South African Astronomical Observatory (SAAO), and we thank R. Manick for his assistance in taking the observations of Hen2-375.

This research has made use of the SIMBAD data base and VizieR catalogue access tool, operated at CDS, Strasbourg, France. It also used observations made with the NASA/ESA *Hubble Space Telescope*, and obtained from the Hubble Legacy Archive, which is a collaboration between the Space Telescope Science Institute (STScI/NASA), the Space Telescope European Coordinating Facility (ST-ECF/ESA) and the Canadian Astronomy Data Centre (CADC/NRC/CSA).

This paper utilizes public domain data obtained by the MACHO Project, jointly funded by the US Department of Energy through the University of California, Lawrence Livermore National Laboratory under contract No. W-7405-Eng-48, by the National Science Foundation through the Center for Particle Astrophysics of the University of California under cooperative agreement AST-8809616, and by the Mount Stromlo and Siding Spring Observatory, part of the Australian National University.

This research has made use of SAO ımage DS9, developed by Smithsonian Astrophysical Observatory, and Montage, funded by the National Aeronautics and Space Administration's Earth Science Technology Office, Computation Technologies Project, under Cooperative Agreement Number NCC5-626 between NASA and the California Institute of Technology. Montage is maintained by the NASA/IPAC Infrared Science Archive.

REFERENCES

Acker A., Stenholm B., 1990, A&AS, 86, 219
Alcock C. et al., 1997, ApJ, 479, 119
Alksnis A., Balklavs A., Dzervitis U., Eglitis I., Paupers O., Pundure I., 2001, Balt. Astron., 10, 1
Allen D. A., 1984, Publ. Astron. Soc. Aust., 5, 369
Azzopardi M., Lequeux J., Rebeirot E., 1985, A&A, 145, L4
Azzopardi M., Rebeirot E., Lequeux J., Westerlund B. E., 1991, A&AS, 88, 265
Babusiaux C., Gilmore G., 2005, MNRAS, 358, 1309
Belczyński K., Mikołajewska J., Munari U., Ivison R. J., Friedjung M., 2000, A&AS, 146, 407
Benjamin R. A. et al., 2003, PASP, 115, 953
Bessell M. S., Germany L. M., 1999, PASP, 111, 1421
Bond H. E., 2009, J. Phys.: Conf. Ser., 172, 012029
Brocklehurst M., 1971, MNRAS, 153, 471
Buckley D. A. H., Swart G. P., Meiring J. G., 2006, Proc. SPIE, 6267, 32
Burgh E. B., Nordsieck K. H., Kobulnicky H. A., Williams T. B., O'Donoghue D., Smith M. P., Percival J. W., 2003, Proc. SPIE, 4841, 1463
Cabrera-Lavers A., Bilir S., Ak S., Yaz E., López-Corredoira M., 2007, A&A, 465, 825
Chesneau O. et al., 2006, A&A, 455, 1009
Churchwell E. et al., 2009, PASP, 121, 213
Cohen M., Barlow M. J., Liu X.-W., Jones A. F., 2002, MNRAS, 332, 879
Cohen M. et al., 2007, ApJ, 669, 343
Cohen M., Parker Q. A., Green A. J., Miszalski B., Frew D., Murphy T., 2011, MNRAS, 413, 514
Condon J. J., Cotton W. D., Greisen E. W., Yin Q. F., Perley R. A., Taylor G. B., Broderick J. J., 1998, AJ, 115, 1693
Corradi R. L. M., 1995, MNRAS, 276, 521
Corradi R. L. M., 2003, in Corradi R. L. M., Mikołajewska J., Mahoney T. J., eds, ASP Conf. Ser. Vol. 303, Symbiotic Stars Probing Stellar Evolution. Astron. Soc. Pac., San Francisco, p. 393
Corradi R. L. M., 2012, Balt. Astron., 21, 32
Corradi R. L. M., Giammanco C., 2010, A&A, 520, A99
Corradi R. L. M., Brandi E., Ferrer O. E., Schwarz H. E., 1999, A&A, 343, 841
Corradi R. L. M. et al., 2008, A&A, 480, 409
Corradi R. L. M. et al., 2010a, A&A, 509, A41
Corradi R. L. M. et al., 2010b, A&A, 509, L9
Corradi R. L. M., Sabin L., Munari U., Cetrulo G., Englaro A., Angeloni R., Greimel R., Mampaso A., 2011, A&A, 529, A56
Crawford S. M. et al., 2010, Proc. SPIE, 7737, 54
Croom S., Saunders W., Heald R., Bailey J., 2005, The 2dfdr Data Reduction System Users Manual (January 2005), available at http://www.aao.gov.au/AAO/2df/aaomega/aaomega.html
Depew K., Parker Q. A., Miszalski B., De Marco O., Frew D. J., Acker A., Kovacevic A. V., Sharp R. G., 2011, MNRAS, 414, 2812
Di Stefano R., 2010, ApJ, 719, 474
Di Stefano R., Orio M., Moe M., eds, 2013, Proc. IAU Symp. 281, Binary Paths to Type Ia Supernovae Explosions. Cambridge Univ. Press, Cambridge
Dilday B. et al., 2012, Sci, 337, 942
Drew J. E. et al., 2005, MNRAS, 362, 753
Ellis G. L., Grayson E. T., Bond H. E., 1984, PASP, 96, 283
Feast M., 2007, in Kerschbaum F., Charbonnel C., Wing R. F., eds, ASP Conf. Ser. Vol. 378, Why Galaxies Care About AGB Stars: Their Importance as Actors and Probes. Astron. Soc. Pac., San Francisco, p. 479
Feast M. W., Whitelock P. A., Carter B. S., 1990, MNRAS, 247, 227
Frew D. J., Parker Q. A., 2010, PASA, 27, 129
Fulbright M. S., Liebert J., 1993, ApJ, 410, 275
Gesicki K., Zijlstra A. A., Szyszka C., Hajduk M., Lagadec E., Guzman Ramirez L., 2010, A&A, 514, A54
Giveon U., Becker R. H., Helfand D. J., White R. L., 2005, AJ, 130, 156
Goeres A., Sedlmayr E., 1992, A&A, 265, 216
Gonzalez O. A., Rejkuba M., Minniti D., Zoccali M., Valenti E., Saito R. K., 2011, A&A, 534, L14
Górny S. K., Stasińska G., Escudero A. V., Costa R. D. D., 2004, A&A, 427, 231
Górny S. K., Chiappini C., Stasińska G., Cuisinier F., 2009, A&A, 500, 1089

Gromadzki M., Mikołajewska J., Whitelock P., Marang F., 2009, Acta Astron., 59, 169
Gutierrez-Moreno A., Moreno H., Cortes G., 1995, PASP, 107, 462
Hajduk M., Zijlstra A. A., Gesicki K., 2008, A&A, 490, L7
Hambly N. C. et al., 2001, MNRAS, 326, 1279
Hambly N., Read M., Mann R., Sutorius E., Bond I., MacGillivray H., Williams P., Lawrence A., 2004, in Ochsenbein F., Allen M. G., Egret D., eds, ASP Conf. Ser. Vol. 314, Astronomical Data Analysis Software and Systems (ADASS) XIII. Astron. Soc. Pac., San Francisco, p. 137
Hamuy M., Suntzeff N. B., Heathcote S. R., Walker A. R., Gigoux P., Phillips M. M., 1994, PASP, 106, 566
Handler G., 2003, in Sterken C., ed., ASP Conf. Ser. Vol. 292, Interplay of Periodic, Cyclic and Stochastic Variability in Selected Areas of the H-R Diagram. Astron. Soc. Pac., San Francisco, p. 183
Henize K. G., 1967, ApJS, 14, 125
Hong J. S., van den Berg M., Grindlay J. E., Laycock S., 2009, ApJ, 706, 223
Jacoby G. H., Van de Steene G., 2004, A&A, 419, 563
Jones A., Lawson W., De Marco O., Kilkenny D., van Wyk F., Roberts G., 1999, The Observatory, 119, 76
Jonker P. G. et al., 2011, ApJS, 194, 18
Jurdana-Šepić R., Munari U., 2010, PASP, 122, 35
Kato M., Hachisu I., Mikołajewska J., 2013, ApJ, 763, 5
Kenyon S. J., 1986, The Symbiotic Stars. Cambridge Univ. Press, Cambridge, p. 295
Kenyon S. J., Fernandez-Castro T., 1987, AJ, 93, 938
Kenyon S. J., Oliversen N. A., Mikołajewska J., Mikolajewski M., Stencel R. E., Garcia M. R., Anderson C. M., 1991, AJ, 101, 637
Kenyon S. J., Livio M., Mikołajewska J., Tout C. A., 1993, ApJ, 407, L81
Kobulnicky H. A., Nordsieck K. H., Burgh E. B., Smith M. P., Percival J. W., Williams T. B., O'Donoghue D., 2003, Proc. SPIE, 4841, 1634
Kohoutek L., 1977, A&A, 59, 137
Kohoutek L., 2002, Astron. Nachr., 323, 57
Kohoutek L., Wehmeyer R., 2003, Astron. Nachr., 324, 437 (KW2003)
Lagadec E. et al., 2006, A&A, 448, 203
Lamers H. J. G. L. M., Zickgraf F.-J., de Winter D., Houziaux L., Zorec J., 1998, A&A, 340, 117
Lenz P., Breger M., 2004, in Zverko J., Ziznovsky J., Adelman S. J., Weiss W. W., eds, Proc. IAU Symp. 224, The A-Star Puzzle. Cambridge Univ. Press, Cambridge, p. 786
Leuenhagen U., Hamann W.-R., Jeffery C. S., 1996, A&A, 312, 167
Lewis I. J. et al., 2002, MNRAS, 333, 279
Liebert J., Green R., Bond H. E., Holberg J. B., Wesemael F., Fleming T. A., Kidder K., 1989, ApJ, 346, 251
Luna G. J. M., Costa R. D. D., 2005, A&A, 435, 1087
Luna G. J. M., Sokoloski J. L., Mukai K., Nelson T., 2012, A&A, preprint (arXiv:1211.6082)
Lutz J. H., Kaler J. B., 1983, PASP, 95, 739
Lutz J., Fraser O., McKeever J., Tugaga D., 2010, PASP, 122, 524
Maercker M. et al., 2012, Nat, 490, 232
Magrini L., Corradi R. L. M., Munari U., 2003, in Corradi R. L. M., Mikołajewska J., Mahoney T. J., eds, ASP Conf. Ser. Vol. 303, Symbiotic Stars Probing Stellar Evolution. Astron. Soc. Pac., San Francisco, p. 539
Matsunaga N., Fukushi H., Nakada Y., 2005, MNRAS, 364, 117
Matsunaga N., Fukushi H., Nakada Y., 2013, MNRAS, 429, 385
Mikołajewska J., 1999, in Guenther E., Stecklum B., Klose S., eds, ASP Conf. Ser. Vol. 188, Optical and Infrared Spectroscopy of Circumstellar Matter. Astron. Soc. Pac., San Francisco, p. 291
Mikołajewska J., 2001, in Paczynski B., Chen W.-P., Lemme C., eds, ASP Conf. Ser. Vol. 246, IAU Colloq. 183: Small Telescope Astronomy on Global Scales. Astron. Soc. Pac., San Francisco, p. 167
Mikołajewska J., 2004, Rev. Mex. Astron. Astrofis. Conf. Ser., 20, 33
Mikołajewska J., 2007, Balt. Astron., 16, 1
Mikołajewska J., 2012, Balt. Astron., 21, 5
Mikołajewska J., 2013, in Di Stefano R., Orio M., Moe M., eds, Proc. IAU Symp. 281, Binary Paths to Type Ia Supernovae Explosions, Proceedings of the International Astronomical Union. Cambridge Univ. Press, Cambridge, p. 162
Mikołajewska J., Kenyon S. J., 1992, AJ, 103, 579
Mikołajewska J., Acker A., Stenholm B., 1997, A&A, 327, 191
Mikołajewska J., Brandi E., Hack W., Whitelock P. A., Barba R., Garcia L., Marang F., 1999, MNRAS, 305, 190
Miroshnichenko A. S., 2006, in Kraus M., Miroshnichenko A. S., eds, ASP Conf. Ser. Vol. 355, Stars with the B[e] Phenomenon. Astron. Soc. Pac., San Francisco, p. 13
Miszalski B., 2009, PhD thesis, Macquarie University and Université de Strasbourg
Miszalski B., Shortridge K., Saunders W., Parker Q. A., Croom S. M., 2006, MNRAS, 371, 1537
Miszalski B., Parker Q. A., Acker A., Birkby J. L., Frew D. J., Kovacevic A., 2008, MNRAS, 384, 525
Miszalski B., Acker A., Moffat A. F. J., Parker Q. A., Udalski A., 2009a, A&A, 496, 813
Miszalski B., Acker A., Parker Q. A., Moffat A. F. J., 2009b, A&A, 505, 249
Miszalski B. et al., 2011a, A&A, 528, A39
Miszalski B., Napiwotzki R., Cioni M.-R. L., Nie J., 2011b, A&A, 529, A77
Miszalski B., Napiwotzki R., Cioni M.-R. L., Groenewegen M. A. T., Oliveira J. M., Udalski A., 2011c, A&A, 531, A157
Miszalski B., Acker A., Parker Q. A., Boffin H. M. J., Frew D. J., Mikolajewska J., Moffat A. F. J., Napiwotzki R., 2011d, in Zijlstra A. A., Lykou F., McDonald I., Lagadec E., eds, Proc. Asymmetric Planetary Nebulae 5 Conference. Jodrell Bank Centre for Astrophysics, Manchester, p. 109
Munari U., Jurdana-Šepić R., 2002, A&A, 386, 237
Munari U., Renzini A., 1992, ApJ, 397, L87
Munari U., Jurdana-Šepić R., Moro D., 2001, A&A, 370, 503
Munari U. et al., 2011, MNRAS, 410, L52
Mürset U., Nussbaumer H., 1994, A&A, 282, 586
Mürset U., Schmid H. M., 1999, A&AS, 137, 473
Mürset U., Wolff B., Jordan S., 1997, A&A, 319, 201
Ng Y. K., 1999, in Le Bertre T., Lebre A., Waelkens C., eds, Proc. IAU Symp. 191, Asymptotic Giant Branch Stars, p. 545
Nicholls C. P., Wood P. R., Cioni M.-R. L., Soszyński I., 2009, MNRAS, 399, 2063
Nowotny W., Aringer B., Höfner S., Eriksson K., 2013, A&A, 552, A20
O'Donoghue D. et al., 2006, MNRAS, 372, 151
Oke J. B., 1990, AJ, 99, 1621
Parker Q. A., Morgan D. H., 2003, MNRAS, 341, 961
Parker Q. A. et al., 2005, MNRAS, 362, 689
Parker Q. A. et al., 2006, MNRAS, 373, 79
Pasquini L. et al., 2002, The Messenger, 110, 1
Pereira C. B., Smith V. V., Cunha K., 2005, A&A, 429, 993
Pigulski A., Kolaczkowski Z., Kopacki G., 2003, Acta Astron., 53, 27
Pojmanski G., 2002, Acta Astron., 52, 397
Poleski R. et al., 2011, Acta Astron., 61, 123
Pollacco D. L., Kilkenny D., Marang F., van Wyk F., Roberts G., 1992, MNRAS, 256, 669
Porter J. M., Rivinius T., 2003, PASP, 115, 1153
Pottasch S. R., Olling R., Bignell C., Zijlstra A. A., 1988, A&A, 205, 248
Proga D., Mikołajewska J., Kenyon S. J., 1994, MNRAS, 268, 213
Rattenbury N. J., Mao S., Sumi T., Smith M. C., 2007, MNRAS, 378, 1064
Richer H. B., 1971, ApJ, 167, 521
Rodríguez M., Corradi R. L. M., Mampaso A., 2001, A&A, 377, 1042
Ruffle P. M. E., Zijlstra A. A., Walsh J. R., Gray M. D., Gesicki K., Minniti D., Comeron F., 2004, MNRAS, 353, 796
Rutkowski A., Mikołajewska J., Whitelock P. A., 2007, Balt. Astron., 16, 49
Samus N. N. et al., 2012, General Catalog of Variable Stars (GCVS database, Version 2012Jan), CDS B/gcvs, avaliable at http://cdsarc.u-strasbg.fr/viz-bin/Cat?B/gcvs
Santander-García M., Rodriguez-Gil P., Jones D., Corradi R. L. M., Miszalski B., Pyrzas S., Rubio-Diez M. M., 2011, in Zijlstra A. A., Lykou F., McDonald I., Lagadec E., eds, Proc. Asymmetric Planetary Nebulae 5 Conference. Jodrell Bank Centre for Astrophysics, Manchester, p. 259

Schmeja S., Kimeswenger S., 2001, A&A, 377, L18
Schmid H. M., 1989, A&A, 211, L31
Schmid H. M., Nussbaumer H., 1993, A&A, 268, 159
Schwarz H. E., Corradi R. L. M., Melnick J., 1992, A&AS, 96, 23
Sharp R. et al., 2006, Proc. SPIE, 6269, 14
Shaw R. A., Wirth A., 1985, PASP, 97, 1071
Shore S. N. et al., 2011, A&A, 527, A98
Shore S. N., Wahlgren G. M., Augusteijn T., Liimets T., Koubsky P., Slechta M., Votruba V., 2012, A&A, 540, A55
Shortridge K., Ramage C., Farrell T., 2006, 2dF/6dF/AAOmega configure User Manual v.1.5, available at http://www.aao.gov.au/AAO/2df/aaomega/aaomega.html
Skrutskie M. F. et al., 2006, AJ, 131, 1163
Smith L. F., Shara M. M., Moffat A. F. J., 1996, MNRAS, 281, 163
Solf J., 1984, A&A, 139, 296
Soszyński I. et al., 2013, Acta Astron., 63, 21
Stanek K. Z., Udalski A., Szymanski M., Kaluzny J., Kubiak M., Mateo M., Krzeminski W., 1997, ApJ, 477, 163
Stellingwerf R. F., 1978, ApJ, 224, 953
Su K. et al., 2011, in Zijlstra A. A., Lykou F., McDonald I., Lagadec E., eds, Proc. Asymmetric Planetary Nebulae 5 Conference. Jodrell Bank Centre for Astrophysics, Manchester, p. 101
Szymański M. K., 2005, Acta Astron., 55, 43
Szymański M. K., Udalski A., Soszynski I., Kubiak M., Pietrzynski G., Poleski R., Wyrzykowski L., Ulaczyk K., 2011, Acta Astron., 61, 83
Tappert C., Ederoclite A., Mennickent R. E., Schmidtobreick L., Vogt N., 2012, MNRAS, 423, 2476
Terzan A., Gosset E., 1991, A&AS, 90, 451
Torres-Peimbert S., Dufour R. J., Peimbert M., Pena M., 1997, in Habing H. J., Lamers H. J. G. L. M, eds, Proc. IAU Symp. 180, Planetary Nebulae. Kluwer, Dordrecht, p. 281
Tuthill P. G., Monnier J. D., Danchi W. C., 1999, Nat, 398, 487
Udalski A., 2009, in ASP Conf. Ser. Vol. 403, The Variable Universe: A Celebration of Bohdan Paczynski. Astron. Soc. Pac., San Francisco, p. 110
Udalski A., Szymański M., Kaluzny J., Kubiak M., Mateo M., 1992, Acta Astron., 42, 253
Udalski A., Kubiak M., Szymański M., 1997, Acta Astron., 47, 319
Udalski A. et al., 2002a, Acta Astron., 52, 1
Udalski A. et al., 2002b, Acta Astron., 52, 217
Udalski A., Szymański M. K., Soszynski I., Poleski R., 2008, Acta Astron., 58, 69
Udalski A. et al., 2012, Acta Astron., 62, 133
Van de Steene G. C., Jacoby G. H., 2001, A&A, 373, 536
van der Hucht K. A., 2001, New Astron. Rev., 45, 135
Veen P. M., van Genderen A. M., van der Hucht K. A., Li A., Sterken C., Dominik C., 1998, A&A, 329, 199
Voges W. et al., 2000, IAU Circ., 7432, 3
Wahlin R., Eriksson K., Gustafsson B., Ryde N., Westerlund B., Lambert D. L., 2007, in Kerschbaum F., Charbonnel C., Wing R. F., eds, ASP Conf. Ser. Vol. 378, Why Galaxies Care About AGB Stars: Their Importance as Actors and Probes. Astron. Soc. Pac., San Francisco, p. 410
Walter F. M., Battisti A., Towers S. E., Bond H. E., Stringfellow G. S., 2012, PASP, 124, 1057
Warner B., 2003, Cataclysmic Variable Stars. Cambridge Univ. Press, Cambridge, UK, p. 592 (ISBN 052154209X)
Westerlund B. E., Lequeux J., Azzopardi M., Rebeirot E., 1991, A&A, 244, 367
Whitelock P. A., 1987, PASP, 99, 573
Whitelock P., 1993, in DeJonghe H., Habing H. J., eds, Proc. IAU Symp. 153, Galactic Bulges. Kluwer, Dordrecht, p. 39
Whitelock P., Menzies J., Irwin M., Feast M., 1999, in Whitelock P., Cannon R., eds, Proc. IAU Symp. 192, The Stellar Content of Local Group Galaxies. Astron. Soc. Pac., San Francisco, p. 136
Whitelock P., Marang F., Feast M., 2000, MNRAS, 319, 728
Whitelock P. A., Feast M. W., Marang F., Groenewegen M. A. T., 2006, MNRAS, 369, 751
Whitelock P. A., Feast M. W., van Leeuwen F., 2008, MNRAS, 386, 313
Woudt P. A., Warner B., Spark M., 2005, MNRAS, 364, 107
Zhang Y., Liu X.-W., 2003, A&A, 404, 545
Zhang Y., Liu X.-W., Luo S.-G., Péquignot D., Barlow M. J., 2005, A&A, 442, 249

APPENDIX A: NEAR-INFRARED AND MID-INFRARED PHOTOMETRY

Table A1. 2MASS and GLIMPSE magnitudes of new and possible symbiotic stars. The full version is available online.

Name	Type	J	H	K_s	$J-H$	$H-K_s$	$J-K_s$	Qflag	[3.6]	[4.5]	[5.8]	[8.0]
000.49−01.45	S	9.86	8.48	7.73	1.38	0.75	2.13	AAA	7.34	7.57	7.28	7.25
001.70−03.67	S	9.00	8.12	7.78	0.88	0.34	1.22	AAA	7.64	7.76	7.62	7.47
002.86−01.88	S	9.98	8.68	8.10	1.30	0.58	1.88	AAA	7.77	7.90	7.69	7.64
...	...	...	...	...	...	...	...	...	...	...	...	...

Table A2. 2MASS and GLIMPSE magnitudes of other objects. The full version is available online.

Name	Type	J	H	K_s	$J-H$	$H-K_s$	$J-K_s$	Qflag	[3.6]	[4.5]	[5.8]	[8.0]
003.16−02.31	Nova	–	–	–	–	–	–	–	13.74	12.75	11.99	10.43
359.88−03.58	WN6	13.72	13.28	12.83	0.44	0.44	0.88	AAA	12.27	11.79	11.56	11.36
H2-32	Be?	13.80	13.43	12.57	0.38	0.86	1.24	AAA	9.80	9.06	8.49	7.57
...	...	...	...	...	...	...	...	...	...	...	...	...

APPENDIX B: ADDITIONAL SPECTROSCOPY

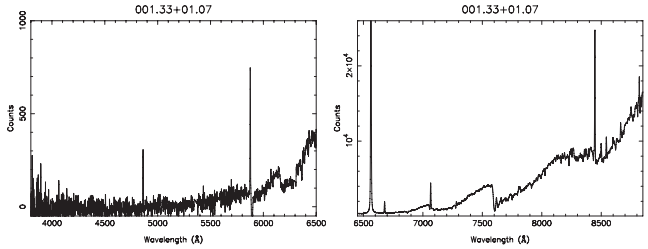

Figure B1. AAOmega spectra of possible S-type symbiotic stars. The full version is available online.

Figure B2. AAOmega spectra of possible S-type symbiotic stars (continuation of Fig. B1). The full version is available online.

Figure B3. AAOmega spectra of possible D-type symbiotic stars. The full version is available online.

Figure B4. AAOmega spectra of possible D-type symbiotic stars (continuation of Fig. B3). The full version is available online.

Figure B5. AAOmega spectra of possible D-type symbiotic stars (continuation of Fig. B4). The full version is available online.

Figure B6. AAOmega spectra of other objects excluding PNe with HDCs (see Fig. 10) and superpositions (see Appendix E). The full version is available online.

Figure B7. AAOmega spectra of other objects (continuation of Fig. B6). The full version is available online.

Figure B8. AAOmega spectra of other objects (continuation of Fig. B7). The full version is available online.

APPENDIX C: LIGHT CURVES

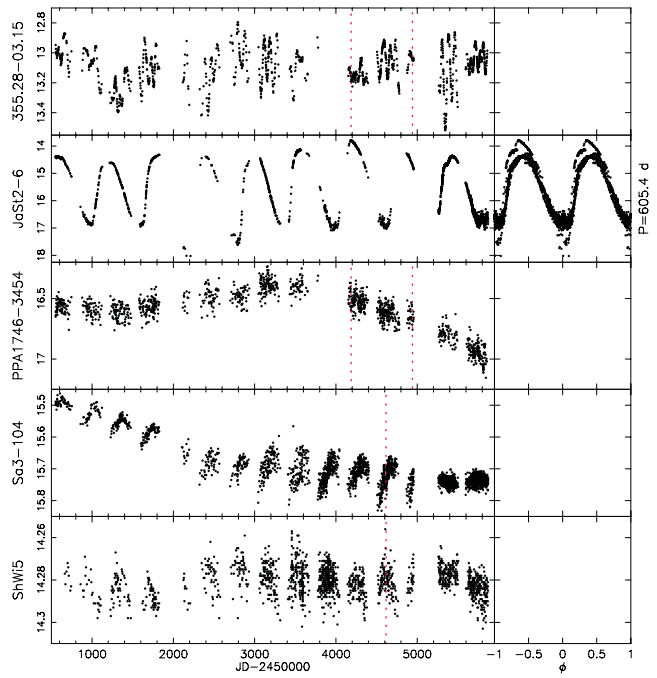

Figure C1. Combined OGLE-II, OGLE-III and OGLE-IV light curves. The full version is available online.

Figure C2. Combined OGLE-III and OGLE-IV light curves of objects not observed during previous OGLE phases. The full version is available online.

Figure C3. Combined OGLE-III and OGLE-IV light curves (continuation of Fig. C2). The full version is available online.

Figure C4. Combined OGLE-III and OGLE-IV light curves (continuation of Fig. C3). The full version is available online.

Figure C5. Combined OGLE-III and OGLE-IV light curves (continuation of Fig. C4). The full version is available online.

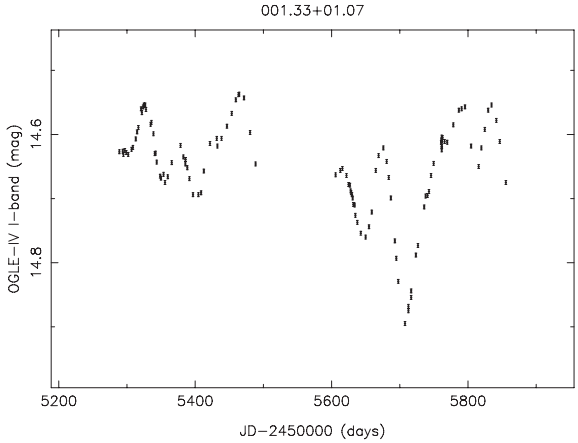

Figure C6. OGLE-IV light curves of objects not observed during previous OGLE phases. The full version is available online.

Figure C7. OGLE-IV light curves (continuation of Fig. C6). The full version is available online.

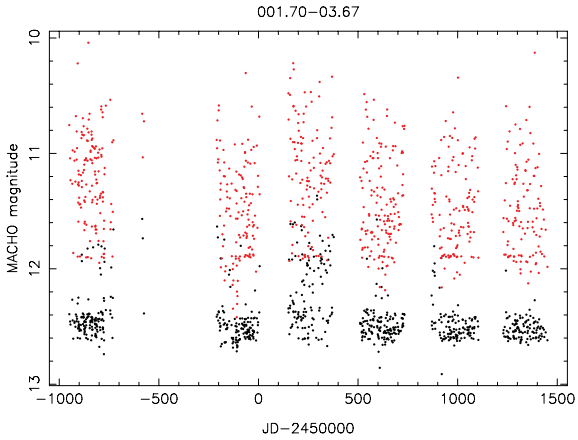

Figure C8. MACHO *V* (black) and *R* (red) light curves. The full version is available online.

APPENDIX D: IMAGES

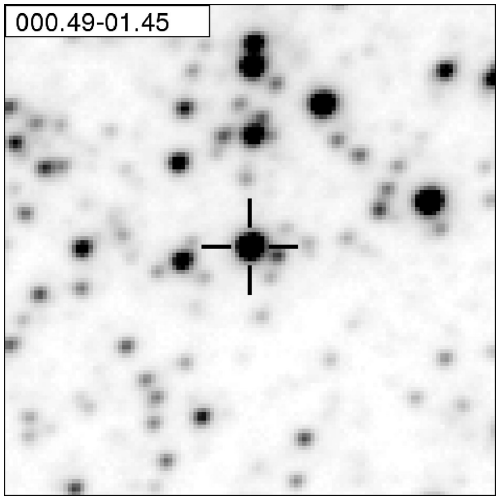

Figure D1. OGLE-III and OGLE-IV *I*-band images. The full version is available online.

Figure D2. OGLE-III and OGLE-IV *I*-band images (continuation of Fig. D1). The full version is available online.

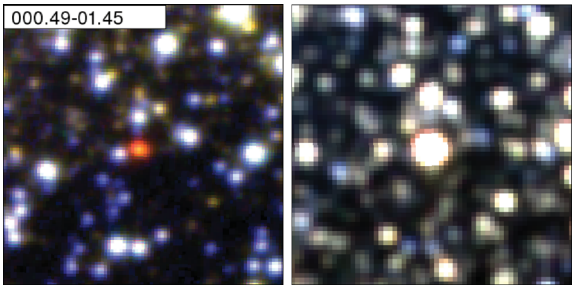

Figure D3. Colour-composite images of our sample. The full version is available online.

Figure D4. Colour-composite images (continuation of Fig. D3). The full version is available online.

Figure D5. Colour-composite images (continuation of Fig. D4). The full version is available online.

Figure D6. Colour-composite images (continuation of Fig. D5). The full version is available online.

Figure D7. Colour-composite images (continuation of Fig. D6). The full version is available online.

APPENDIX E: SUPERPOSITIONS

The full text of this section is available online.

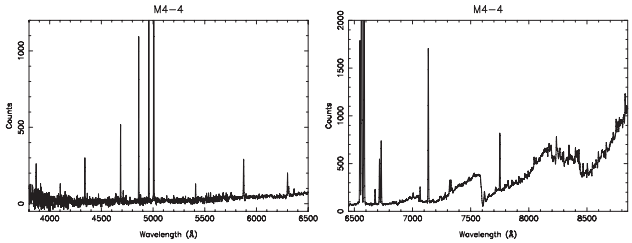

Figure E1. Spectra of two superpositions. The full version is available online.

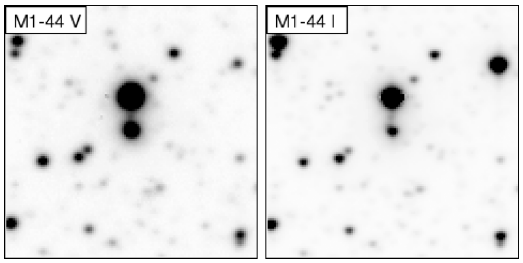

Figure E2. Images of superpositions in bulge PNe. The full version is available online.

SUPPORTING INFORMATION

Additional Supporting Information may be found in the online version of this article:

APPENDIX A: Near-infrared and mid-infrared photometry
APPENDIX B: Additional spectroscopy
APPENDIX C: Light curves
APPENDIX D: Images

APPENDIX E: Superpositions (http://mnras.oxfordjournals.org/lookup/suppl/doi:10.1093/mnras/stt673/-/DC1).

Please note: Oxford University Press are not responsible for the content or functionality of any supporting materials supplied by the authors. Any queries (other than missing material) should be directed to the corresponding author for the article.

This paper has been typeset from a TEX/LATEX file prepared by the author.